Energy-resolved study of the spin precession in photoemission from activated (110) GaAs

H. Riechert*
Institut für Festkörperforschung der Kernforschungsanlage Jülich, D-5170 Jülich, West Germany

H.-J. Drouhin and C. Hermann
Laboratoire de Physique de la Matière Condensée, Ecole Polytechnique, 91128 Palaiseau, France
(Received 7 March 1988)

The measurement of the spin vector **S** of electrons photoemitted from a III-V compound semiconductor activated to negative electron affinity is shown to be a powerful means to explore band hybridization properties, surface effects, and to estimate characteristic times of electron relaxation. Because of the lack of inversion symmetry (i.e., to the conduction-band spin splitting), an internal spin precession occurs in the bulk semiconductor and also in the band-bending region (BBR) near the surface. From the modulus of **S** we determine the hot-electron mean free path. From the **S** direction we deduce the angle of spin precession θ_p due to the internal precession vector ω. The experimental originality of the present work stands in the combination of the **S** measurement with the high-resolution energy analysis of the photoemitted electrons. The dependence of θ_p on the electron kinetic energy reflects the memory of the initial anisotropic distribution of electron momenta, and its modifications during thermalization and transit through the BBR. Our analysis relates the D'ymnikov-D'yakonov-Perel' formalism for the calculation of spin-polarization properties under circularly polarized light excitation with the widely used Kane $\mathbf{k}\cdot\mathbf{p}$ band description.

I. INTRODUCTION

Because of the lack of inversion symmetry in III-V semiconducting compounds, the spin degeneracy of the conduction band is lifted.[1] This fact can be described by a perturbation Hamiltonian $H=\mathbf{S}\cdot\omega(\mathbf{k})$, which defines an internal precession vector $\omega(\mathbf{k})$, of cubic symmetry, a function of the wave vector **k**, and acting on the spin vector **S** (throughout this paper vectors are designated by boldface characters, their moduli by plain characters). Since this precession in the semiconductor leads to spin relaxation,[2] the properties of $\omega(\mathbf{k})$ have been first investigated in polarized photoluminescence experiments.[3] More recently, this precession vector was directly evidenced in a photoemission experiment performed on thermalized spin-polarized electrons in *p*-type GaAs with a (110) surface, activated to negative electron affinity (NEA) by cesium and oxygen co-adsorption.[4,5] The principle of this experiment is the following: absorption of circularly polarized light with an energy $h\nu$ close to the band-gap energy E_G excites spin-polarized electrons into the conduction band. By ballistically traveling towards the surface through the *band-bending region* (BBR), all thermalized electrons gain the same momentum **k** normal to the surface, and suffer the same spin precession. Thereby the net spin momentum vector is rotated away from its initial direction. The total precession angle θ_p is then compensated for by application of an external magnetic field. Such an experiment leads to combined information on the magnitude of the internal precession vector $\omega(\mathbf{k})$ and on the band-bending (BB) energy δ.

The role of $\omega(\mathbf{k})$ was also pointed out in a different spin-polarized photoemission experiment on NEA GaAs, with a (100) surface, and exciting photon energies $h\nu > E_G$:[6] the photoemitted ballistic electrons originate from a hot-electron mean free path l inside the solid; during their transit towards the surface they experience a spin precession which depends on their momentum orientation. The average spin vector and, consequently, the hot-electron polarization measured in photoemission are reduced by this effect, which essentially arises from the *bulk* precession, since l ($\approx$1000 Å) is much larger than the BB width [$\approx$100–300 Å for a *p*-type doping in the (10^{19}–10^{18})-cm^{-3} range]. This yields an estimate of $\omega(\mathbf{k})$ together with l.

The analysis of the high-resolution (20-meV) energy-distribution curves (EDC's) from NEA GaAs(100) was shown to allow a precise exploration of the band structure.[7] The EDC results are completed by the measurement of the emitted electron polarization, P, versus the kinetic energy, ε, in the conduction band [polarization versus energy distribution curves (PEDC's)]: such studies provide information on the band hybridization and the thermalization of the photoexcited electrons in the conduction band.[6] In the present paper we use the same energy-analysis technique to obtain the internal precession angle $\theta_p(\varepsilon)$ versus the electron kinetic energy at a given $h\nu$, and get a direct picture of the evolution of the electron spin. The whole precession effect is due to the existence of the precession vector $\omega(\mathbf{k})$, whose basic properties in the vicinity of the zone center are recalled here.[2]

(i) $\omega(\mathbf{k})$ is perpendicular to **k**.

(ii) $\omega(\mathbf{k})$ is highly anisotropic, it is zero for **k** along all ⟨100⟩ and ⟨111⟩ directions and maximum for **k** along ⟨110⟩ directions,

(iii) The components of $\omega(\mathbf{k})$ are increasing with ε.

Consequently, spin precession occurs in two distinct regions: the bulk solid, where the kinetic energy at creation can be reduced by energy relaxation, and the band bending region, in which the kinetic energy, and consequently ω, increase during the transport towards the surface (in this latter region, relatively narrow in the heavily doped samples used for NEA photoemission, collisions are improbable, and the transport is ballistic). Thus the measured precession angle combines bulk and band-bending effects, and contains information on the degree of electron thermalization. These different contributions are disentangled by the energy-analysis technique.

Section II is devoted to the description of the experiment, Sec. III to the detailed theoretical principles: in particular, we relate the D'ymnikov-D'yakonov-Perel' (DDP) (Ref. 8) and Kane (Ref. 1) formalisms used in polarization calculations. The analysis of the experimental results in Sec. IV distinguishes between the different features of the precession effect, and leads to the determination of several bulk and band-bending parameters.

II. EXPERIMENT

This paper is focused on the energy-analyzed precession results. Energy-integrated measurements of the precession angle have been published elsewhere.[5,9]

A. Experimental setup

The experimental setup, schematized in Fig. 1, only differs from that described in Refs. 6 and 7 by the precession-angle–measurement apparatus; therefore, we will only recall its essential features and detail its specificities.

The experiment is performed in a ultrahigh-vacuum chamber (pressure $\sim 1\times 10^{-10}$ Torr). A p-type doped GaAs sample is activated to NEA by Cs and O_2 coadsorption according to a standard procedure,[7] and can be cooled down to 110 K by liquid-nitrogen circulation. Electron excitation from one of the three upper valence bands is performed by illumination through a He-Ne laser ($h\nu = 1.96$ eV) or one of the lines of a Kr^+ laser ($1.55 \leq h\nu \leq 3.50$ eV). The exciting beam is circularly polarized through a Babinet-Soleil compensator, so that at excitation the photoexcited-electron mean spin is oriented along the direction z of the incident light; with respect to this direction the electron polarization is defined by $P=(n_+ - n_-)/(n_+ + n_-)$, where n_+ (n_-) is the number of electrons with spin up (down).

To allow magnetic studies, the entire electron optics is of electrostatic type and permits spin-polarization conversion from longitudinal to transverse. The photoemitted electrons are first deflected by a rotator, then energy-selected by a selector operated in the constant-energy mode, with an energy resolution $\Delta E \approx 20$ meV.[10] Then, either they are collected in a Faraday cup, which provides the EDC's, or transported to a Mott polarimeter with concentric electrode geometry,[11] in which their spin polarization is measured.

The sample used for the present experiment is a (110) GaAs crystal (Zn-doped, $p = 1.3\times 10^{18}$ cm^{-3}), cut in the same wafer as that studied in Ref. 9, which was shown to produce large precession effects.

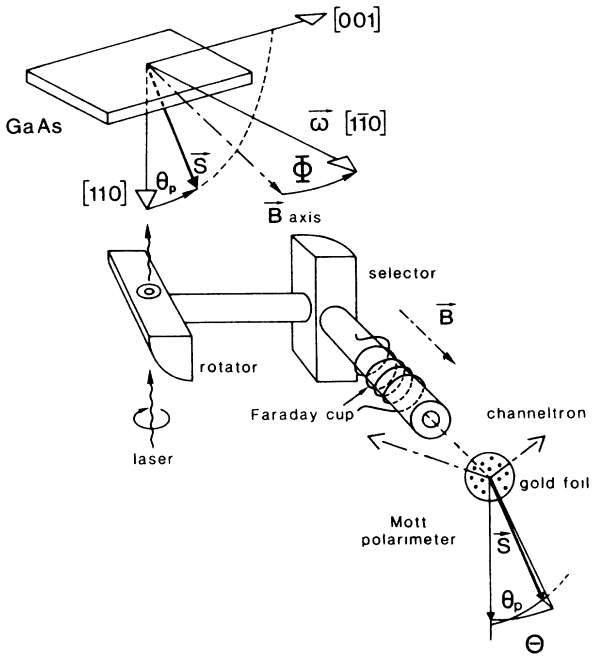

FIG. 1. The central part of the figure schematizes the light-excitation and energy-selection systems. The electrons, deflected by the rotator and energy-analyzed in the selector, can be collected in the Faraday cup, or they can be transported towards the Mott polarimeter, where they are diffused on the gold foil and counted on symmetrical channeltrons. A magnetic field **B** is applied on a part of the electron path. The upper part of the figure defines the orientation in the sample plane with respect to **B**, as given by the angle Φ, and shows the spin momentum **S** after the internal precession due to ω. The lower part of the figure shows that, in the case $\Phi \neq 0$, only partial compensation of θ_p is achieved by the external precession in **B**.

B. Measurement of the precession angle

From the instant of their creation until their emission into vacuum the electrons undergo spin precession due to the presence of $\omega(\mathbf{k})$. For a momentum along [110], i.e., parallel to the light-propagation direction (z axis), ω lies along the [1$\bar{1}$0] direction (see Sec. III B). When all photoelectrons are considered, the average spin vector is rotated by an angle θ_p in the (1$\bar{1}$0) plane (see the discussion in Sec. III). This angle is measured by compensation through an external magnetic field **B** parallel to the propagation direction of the electron beam at the entrance of the Mott polarimeter. Thereby the spin vector along the z direction, which is the polarization component measured in the Mott polarimeter, is maximized.

The compensating field **B** acts on free electrons with mass m and kinetic energy eV (e is the electron charge and V the electrostatic potential), and is obtained by application of a current of intensity i into an N-loop solenoid (Fig. 1). The resulting external precession angle Θ is approximately given by[12]

$$\Theta \approx (\mu_0 \mu_B/\hbar)(2m/eV)^{1/2} Ni = 2\pi i/i_0 \ , \quad (1)$$

where μ_0 is the vacuum permittivity and μ_B the Bohr magneton. The electron energy is ≈ 900 eV, and we use a coil with $N=63$, so that for $\Theta = 2\pi$ we expect $i = i_0 \approx 8$ A. In all our experiments we find $i_0 = 10.2 \pm 0.2$ A, a value which is determined by calibration on (100) GaAs, as shown in Fig. 2. This figure evidences a slight disorientation $\Psi \approx -9°$, in the plane perpendicular to **B**, of the Mott-polarimeter axis relative to the light-propagation direction.

To achieve total compensation of the internal precession, the $[1\bar{1}0]$ direction has to lie parallel to **B**. In our experiment, the sample is rotated in its plane and, for each position, defined by the angle Φ between $[1\bar{1}0]$ and **B**, a variation $P_\Phi(i)$ is expected:

$$P_\Phi(i) = P_0(\Phi)\cos[(2\pi i/i_0) + \xi(\Phi) + \Psi] \ , \quad (2)$$

where $\xi(\Phi)$ and $P_0(\Phi)$ are, respectively, defined by

$$\begin{aligned} &\tan[\xi(\Phi)] = \cos\Phi \tan\theta_p \ , \\ &P_0(\Phi) = P_0(\cos^2\theta_p + \cos^2\Phi \sin^2\theta_p)^{1/2} \ . \end{aligned} \quad (3)$$

Therefore the procedure to measure θ_p is the following.

(i) For a given crystal position, determined by Φ, the polarization is measured versus B, i.e., versus the intensity i in the coil. From a least-squares fit of five or eleven experimental points with Eq. (2), we deduce the "apparent precession angle" $\xi(\Phi)+\Psi$ and $P_0(\Phi)$.

(ii) The experiment is repeated for six crystal positions, obtained by rotation of the crystal around its normal. Measured versus Φ, the angle $\xi(\Phi)+\Psi$ is maximum for $\cos\Phi = 1$, that is, when $[1\bar{1}0]$ is parallel to **B** (see Fig. 3), and is then equal to $\theta_p + \Psi$. In this same position of total compensation of the internal precession by the external magnetic field, we obtain the maximum polarization P_0. By rotation of 180° of the sample around its normal, the internal precession is reversed in the laboratory frame. Because of the disorientation between the Mott-detector axis and the light-propagation direction, under such a rotation the measured angle $\theta_p + \Psi$ is changed into $-\theta_p + \Psi$ (see Figs. 3 and 4), which allows one to eliminate this instrumental asymmetry and to determine the precession angle θ_p. From now on, we discuss measurements taken at $\Phi = 0$, i.e., in a position of total compensation of the internal precession, for which $[1\bar{1}0]$ and **B** are parallel, defining the **y** axis.

Since the precession angle θ_p is calculated through the fitting procedure mentioned above, the evaluation of the uncertainty $\Delta\theta_p$ is somewhat intricate. However, it is straightforward to show that $\Delta\theta_p$ should be proportional to $\Delta P/|P_0|$, where ΔP is the uncertainty on the polarization measurement.[13] This relation stresses that precession angles calculated for small $|P_0|$'s suffer large inaccuracies. To be more quantitative, in the measurements reported in this paper, P_0 is of the order of 10% in cases of weak electron currents (hot electrons) and of a few percents for the stronger currents arising from thermalized electrons. Our Mott detector measures the polarization of a 10-pA beam (to compare with 5 nA, the peak selector output current) with a statistical error of 1% in about 10 min.[6] Under these conditions, the determination of θ_p within $(\Delta\theta_p)° \sim (180/\pi)[1/P_0(\%)] \sim 6°$ requires at least 50 min. Practically, the total experiment time is limited to 6–8 h since the time constant for photocurrent decrease is 3–4 h at 110 K (a few days at 300 K). Therefore during one low-temperature experiment it is only possible to obtain the whole $\theta_p(\varepsilon)$ spectrum for a single value of $h\nu$.

Before presenting the $\theta_p(\varepsilon)$ curves it is interesting to briefly comment on the EDC's taken on the same sample and to compare them to the results published on (100) GaAs.[7]

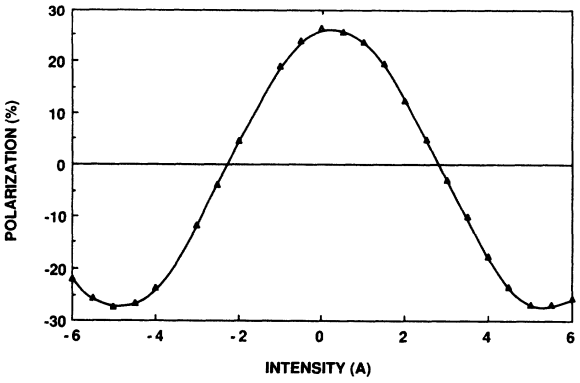

FIG. 2. Variation of the measured polarization vs the intensity in the coil producing the compensating magnetic field **B**. The experiment is performed on (100) GaAs. The experimental asymmetry Ψ appears in the fact that the maximum of the curve occurs for nonzero intensity. The solid line is the best fit to the experimental data according to Eq. (2): $P(\%) = 26.8\cos[360(i/10.3) - 9.3]$, where i is in amperes and the phase in degrees. This gives $\Psi = -9° \pm 1°$.

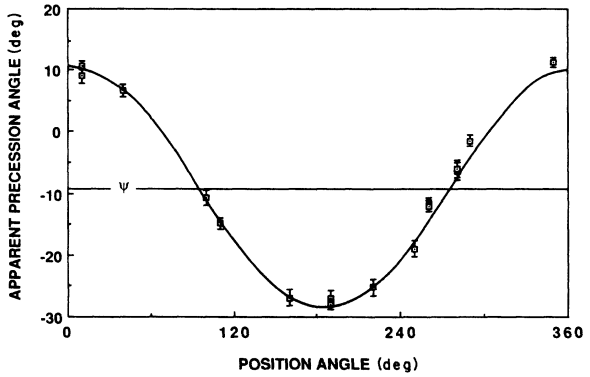

FIG. 3. Experimental variation of the "apparent precession angle" $\xi(\Phi)+\Psi$ vs the angle of rotation Φ specifying the position of the sample in its plane. The solid line is the fit to the relation given in Eq. (3): $\tan\xi(\Phi) = \cos\Phi \tan 19.3°$, for the same experimental asymmetry $\Psi = -9°$ as in Fig. 2. A precession angle of $-19° \pm 1°$ is thus deduced from this curve.

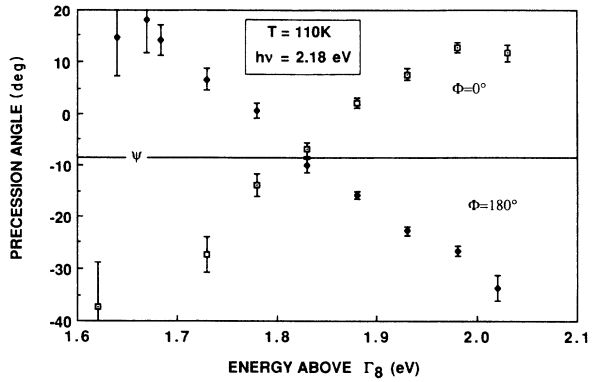

FIG. 4. Raw data of precession-angle measurements taken at $T=110$ K for an excitation energy $h\nu=2.18$ eV. The experimental asymmetry is eliminated by a 180° rotation of the sample.

C. EDC measurements

The EDC's are systematically recorded before and after spin-precession measurements and are used for energy calibration. The principle has been exposed in Ref. 7: at a given excitation energy the high-energy edge of the EDC is due to ballistic electrons excited from the Γ_{8h} heavy-hole valence band. *At low temperature,* this gives rise to a sharp threshold because the probability of energy gain through phonon absorption is negligible. From this threshold the location of the bulk conduction Γ minimum is obtained by subtraction of the kinetic energy at excitation calculated in Kane's anisotropic $\mathbf{k}\cdot\mathbf{p}$ model (the heavy-hole band is taken as anisotropic, the conduction and light-hole ones as isotropic), which gives results comparable to those of pseudopotential or self-consistent linear-muffin-tin-orbital (LMTO) calculations when our experimental resolution is taken into account[14] (to help the interpretation of the experimental data, the electron-excitation energies in the conduction band by optical transitions from the three valence bands, for $T=300$ and 110 K, are given in Table I). The independence of the Γ location with $h\nu$ provides a test of this determination. The Γ location at 300 K can be deduced from its 110-K determination: the displacement essentially comes from the 50-meV Fermi-energy shift towards higher energy (calculated after Ref. 15). The low-energy threshold of the EDC is due to the affinity cutoff. Its position relative to Γ determines the affinity value.

The EDC's on the (110) $p=1.3\times10^{18}$ cm^{-3} sample (Fig. 5) look relatively similar to those measured on (100) GaAs crystals of higher doping level ($p\approx10^{19}$ cm^{-3}). They also evidence several structures, related to the final states of the optical transitions or to conduction-band minima. The main fraction of the corresponding electrons appears down-shifted by a few hundreds of meV in the EDC because of energy loss prior to emission.[7] However, the EDC's for these two crystals differ in two aspects.

(i) As in (100) GaAs, the affinity is negative at room temperature, but in the present case it is close to zero or positive at 110 K. This large change (0.18–0.25 eV) occurs during the short cooling time (≈10 min). It is difficult to attribute it to surface pollution, responsible for the longer (several hours, see Sec. II B) time constant for photocurrent decrease. This variation of electron affinity is comparable to the modification in band bending with temperature (~0.3 eV) observed on this sample, which will be discussed in Sec. IV A.

(ii) All structures are less apparent (see Fig. 5). The Γ peak, which arises from low-energy electrons having lost some energy in the BBR, is broadened for lower doping level, as reported in Ref. 16. These authors, who measure the EDC by the retarding-field technique, observe an L structure only for $N_A\geq5\times10^{18}$ cm^{-3}. They attribute this behavior to the longer energy-relaxation length in the less-doped samples. This should also enhance the hot-electron structures; however, in our case a blurring is observed for the structures associated with electrons relaxed in the conduction-band minima (Γ,L), and also for the hot-electron structures. A possible explanation, not considered in this reference, is that, when decreasing N_A, a more important fraction $\mathcal{L}\alpha(h\nu)$ of the photoelectrons is excited in the wider BBR, of width $\mathcal{L}$, by absorption of light with an absorption coefficient $\alpha(h\nu)$:

$$\mathcal{L}=(2\epsilon_0\epsilon_r\delta/N_Ae^2)^{1/2}\ , \tag{4}$$

where $\epsilon_0\epsilon_r$ is the dielectric constant and δ the BB energy. These electrons have less energy above the Fermi level than those excited in the bulk crystal. The EDC structures should then broaden, especially for larger $h\nu$, because of the increase in α. Indeed, we have observed such a broadening on the heavily p-type doped crystal

TABLE I. Energies (in eV) after excitation into the conduction band from the three valence bands by different krypton and helium-neon laser lines.

		$h\nu$ (eV)							
		1.55	1.65	1.83	1.92	1.96	2.18	2.34	2.60
$T=300$ K	Excitation from Γ_{8h}	1.540	1.625	1.782	1.855	1.890	2.065	2.185	2.395
	Excitation from Γ_{8l}	1.495	1.555	1.670	1.730	1.755	1.912	2.032	2.240
	Excitation from Γ_7			1.470	1.532	1.560	1.680	1.768	1.910
$T=110$ K	Excitation from Γ_{8h}	1.542	1.638	1.795	1.873	1.905	2.080	2.205	2.410
	Excitation from Γ_{8l}	1.531	1.590	1.700	1.760	1.780	1.937	2.045	2.257
	Excitation from Γ_7				1.558	1.583	1.717	1.808	1.945

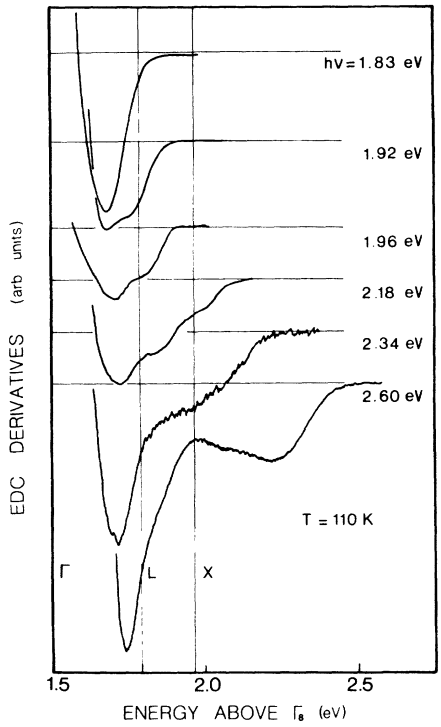

FIG. 5. High-energy part of the EDC derivatives taken at 110 K. The low-energy "Γ peak" is omitted for clarity. The energy resolution is 20 meV.

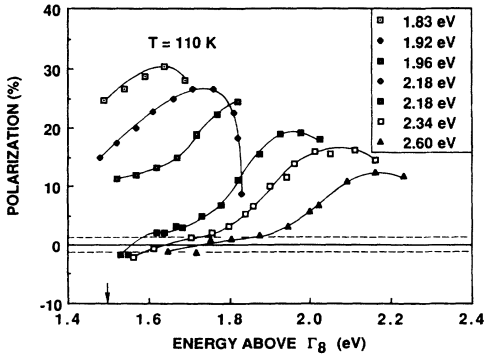

FIG. 6. Measured PEDC's at $T=110$ K, for different excitation energies. In this and the following figures the arrow indicates the location of the bulk conduction-band minimum. The two dashed lines limit the domain in which overly small polarizations prevent precession-angle measurements.

studied in Ref. 7 ($N_A \approx 1\times10^{19}$ cm^{-3}, $\mathcal{L}\approx100$ Å) for $h\nu=3.5$ eV, corresponding to $\alpha\approx7\times10^5$ cm^{-1},[17] $\mathcal{L}\alpha=0.7$. In the EDC's obtained on the present sample ($\mathcal{L}\approx300$ Å) for $h\nu=2.60$ eV ($\alpha\approx2.5\times10^4$ cm^{-1}), the fraction $\mathcal{L}\alpha=7.5\times10^{-2}$ is smaller, but the effect should still be present. Another explanation arises from the energy loss in the BBR, which can only occur by emission of optical phonons, because of carrier depletion in this region. In the random walk of electrons towards the surface, more steps are necessary to cross the wider BBR of the less-doped sample—this should broaden the energy distribution.

D. Polarization versus energy-distribution curves at a given $h\nu$

PEDC's at a given $h\nu$ are obtained from the Mott-detector measurements after *total* compensation of the internal precession by the external magnetic field. They look rather similar (see Fig. 6) to those reported in Ref. 7. Measured against the electron kinetic energy, the spin polarization P_0 shows a high-energy plateau, and a decrease for smaller ε. The plateau arises from ballistic electrons excited with the same photon energy $h\nu$ from different regions of the anisotropic valence band, the largest kinetic energy being carried by electrons with momenta along $\langle 111\rangle$.[17] The maximum P_0 value is reduced when $h\nu$ increases.

E. Energy dependence of the spin precession at a given $h\nu$

The experiment gives the variation, for a given photon energy $h\nu$, of the spin precession θ_p versus the emitted electron kinetic energy ε. The energy resolution is 20 meV. As a test of the crystal orientation we verify that the [001] cleavage directions are properly oriented in the surface plane: this is indeed the case within ±3°. The $\theta_p(\varepsilon)$ spectra reproduced in Fig. 4 are deduced from two measurements corresponding to $[1\bar{1}0]$ parallel and antiparallel to **B**, as explained in Sec. II B. All the following spectra are averages over several runs and are corrected for the experimental asymmetry. Typical results for polarization and precession measurements versus kinetic energy are presented in Fig. 7.

Measurements are performed at 300 and 110 K. At 300 K the curves $\theta_p(\varepsilon)$ obtained for $h\nu=1.55$, 1.83, and 1.92 eV are represented in Fig. 8. Note that the affinity is negative, and that θ_p, which is almost independent of ε for near-band-gap excitation at 1.55 eV ($\theta_p\approx18°$), decreases to zero with ε for $h\nu=1.83$ and 1.92 eV. An overly weak polarization prevents precession measurements for $h\nu>1.96$ eV, as well as in the low-energy part of the EDC's for $h\nu=1.83$ and 1.92 eV.

Results obtained at 110 K for $1.83\leq h\nu\leq2.60$ eV are plotted in Figs. 9 and 10. In these experiments the affinity is nearly zero, so that near band-gap excitation cannot produce significant photoemission (remember that the main Γ peak is usually down-shifted in energy in the BBR, see Ref. 7). A characteristic feature of these $\theta_p(\varepsilon)$ curves is that for high kinetic energies θ_p is positive ($\sim10°$), for intermediate energies it becomes large and negative ($\sim-30°$), and for almost thermalized electrons it is again positive.

To analyze these results we need to elaborate on a model that accounts for the bulk and BB precessions. Therefore, in Sec. III, we detail the expressions of the precession vector $\omega(\mathbf{k})$ acting on the spin of the photoexcited conduction electrons, and take into account the peculiarities of the III-V–compound semiconductor band

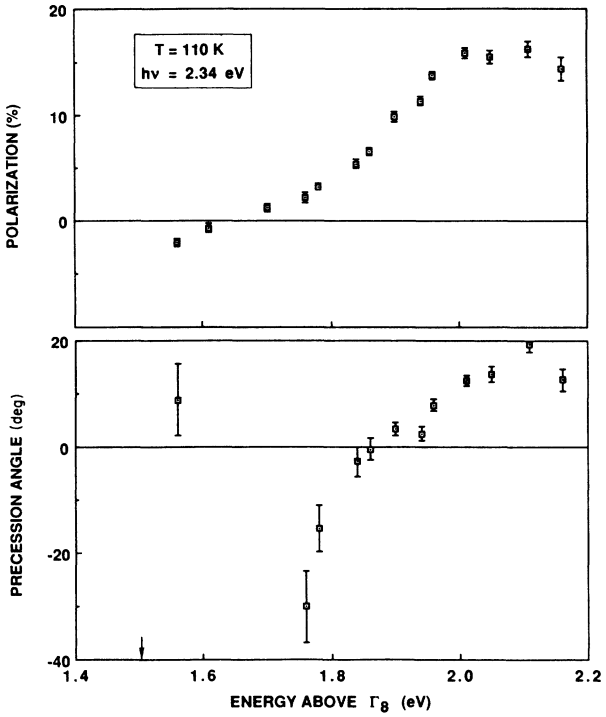

FIG. 7. Typical PEDC and θ_p curves for $T=110$ K, $h\nu=2.34$ eV.

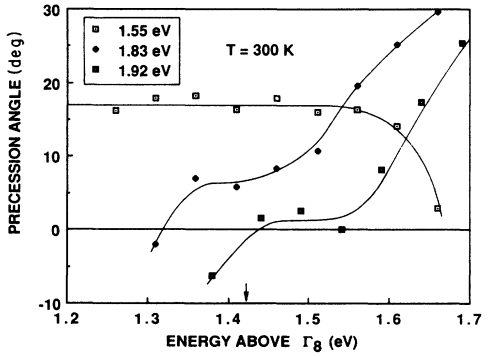

FIG. 8. Precession angle vs the electron energy at $T=300$ K, for the excitation energies $h\nu=1.55$, 1.83, and 1.92 eV.

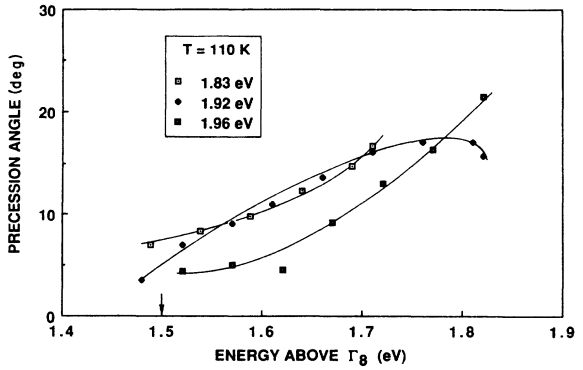

FIG. 9. Precession angle vs the electron energy at $T=110$ K, for the excitation energies $h\nu=1.83$, 1.92, and 1.96 eV.

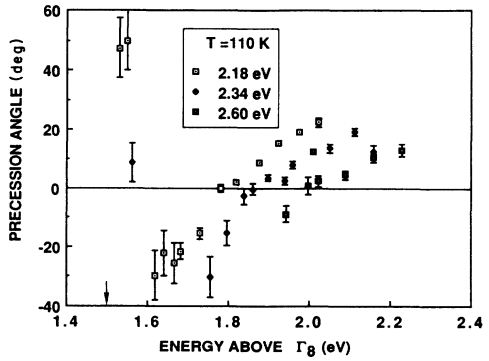

FIG. 10. Precession angle vs the electron energy at $T=110$ K, for the excitation energies $h\nu=2.18$, 2.34, and 2.60 eV.

structure. In Sec. IV we analyze our experimental data in this framework.

III. MODEL FOR ELECTRON-SPIN PRECESSION

The interpretation of the energy-resolved precession measurements is more intricate than that of the original integrated precession experiment performed on thermalized electrons excited by photons of energy $h\nu\approx E_G$.[5] In the latter case, the electron momenta, with negligible value in the bulk crystal, all increase parallel to the normal to the surface in the BBR and are submitted to the same precession vector parallel to **y** so that

$$\theta_p=\int_0^{\tau}\omega_y dt \ , \tag{5}$$

where τ is the electron time of flight across the BBR.

In the present paper the situation is different: the electrons observed through photoemission are excited into the conduction band at high kinetic energy, and travel through the BBR towards the surface, after energy loss inside the bulk crystal for most of them. During their stay in the solid their spins precess in the local $\omega(\mathbf{k})$, which is affected by the **k** modification in the electron motion. In the bulk solid two electron behaviors are possible: (i) the electron momentum **k** is modified in the numerous scatterings, so that $\omega(\mathbf{k})$ changes at each collision. The net effect is a spin depolarization, the so-called D'yakonov-Perel' mechanism,[2] currently observed in polarized luminescence experiments. (ii) Electrons not too distant from the surface travel towards vacuum ballistically; a coherent precession occurs, both in the bulk solid and in the BBR. Because of the increase in momentum along the normal to the surface in the BBR, the precession vector continuously varies along the electron path.

In the following we show that the whole set of observed variations of $\theta_p(\varepsilon)$ for different photon energies can be analyzed with the aid of only two parameters, namely the band-bending energy δ and the hot-electron mean free path $l(\varepsilon)$. We first give some considerations on the value of the spin vector $\mathcal{S}_0(\mathbf{k})$ at excitation, and on the magnitude of $\omega(\mathbf{k})$. Then we describe the different contributions to the observed precession.

A. The spin vector $\mathcal{S}(\mathbf{k})$

In our experiment, spin orientation of conduction electrons is achieved by $\sigma^{\pm}$ circularly-polarized-light excitation, i.e., optical pumping.[18] The electron-density matrix *at excitation* $\underline{\mathbf{F}}$, given by D'ymnikov, D'yakonov, and Perel',[3,8] can be generalized to account for the conduction wave-function modification for $\mathbf{k}\neq 0$ by $\mathbf{k}\cdot\underline{\mathbf{p}}$ perturbation (operators are printed with underlined characters). The calculation is presented in Appendix A, here we only summarize the main results.

The light excitation is normal to the surface, along the z axis. We consider electrons in a $z=$const plane, i.e., we do not take into account the z-dependent absorption process (this effect will be discussed below in Sec. III C 1). Using $\underline{\mathbf{F}}$ and the Pauli operator $\underline{\boldsymbol{\sigma}}=(\underline{\sigma}_x,\underline{\sigma}_y,\underline{\sigma}_z)$, we calculate the momentum distribution $n(\mathbf{k})$ and the electron-spin vector at excitation $\mathcal{S}_0(\mathbf{k})$:

$$n(\mathbf{k})=\mathrm{Tr}\underline{\mathbf{F}},\quad \mathcal{S}_0(\mathbf{k})=\mathrm{Tr}(\underline{\boldsymbol{\sigma}}\,\underline{\mathbf{F}})/\mathrm{Tr}\underline{\mathbf{F}}\ . \tag{6}$$

According to Appendix A, at promotion into the conduction band the spin vector $\mathcal{S}_0(\mathbf{k})$ is a function of $\mathbf{k}$ and is made up of two components: one parallel to $\mathbf{k}$ and the other along z. For an electron promoted from the Γ_{8h} heavy-hole valence band, the only spin component is along $\mathbf{k}$; both components exist in the case of an electron promoted from the Γ_{8l} light-hole or Γ_7 spin-orbit-split bands. During thermalization, the conduction electrons lose correlation between momentum and spin, so that the spin vector, whose modulus decreases because of spin relaxation, lines up along z.

B. The internal precession vector $\omega(\mathbf{k})$

The spin-dependent part of the Hamiltonian[1,2]

$$H=(\hbar/2)\underline{\boldsymbol{\sigma}}\cdot\boldsymbol{\omega}(\mathbf{k}) \tag{7}$$

defines a precession vector $\boldsymbol{\omega}(\mathbf{k})$ with cubic symmetry in the Γ valley: $\boldsymbol{\omega}(\mathbf{k})=\gamma\mathbf{h}(\mathbf{k})$, where $\mathbf{h}(\mathbf{k})$ is normal to $\mathbf{k}$ and related to the $\mathbf{k}$ components (k_x,k_y,k_z) referred to the cubic crystallographic axes by

$$\mathbf{h}(\mathbf{k})=(k_x(k_y^2-k_z^2),\,k_y(k_z^2-k_x^2),\,k_z(k_x^2-k_y^2))\ . \tag{8}$$

For $\mathbf{k}$ along [110], ω is maximal with a modulus equal to $(\gamma k^3)/2=\omega_0$. A LMTO calculation of ω along the [110] direction through the whole Brillouin zone was published in Ref. 19. Having used Kane's $\mathbf{k}\cdot\underline{\mathbf{p}}$ description of the band structure, we instead take the corresponding expression of $\omega(\mathbf{k})$,[1] which has the advantage of allowing analytical calculations along any direction:

$$\omega(\mathbf{k})=4\sqrt{2}(ab/\hbar k)G\mathbf{h}(\mathbf{k})\ . \tag{9}$$

The coefficients a and b are Kane's coefficients for the conduction-band wave functions referred to the $\mathbf{k}$ direction:

$$\phi_{6-}=a\,|\,[iS\downarrow]')+b\,|\,[(X-iY)\uparrow/\sqrt{2}]')+c\,|\,[Z\downarrow]')\ , \tag{10}$$

$$\phi_{6+}=a\,|\,[iS\uparrow]')+b\,|\,[-(X+iY)\downarrow/\sqrt{2}]')+c\,|\,[Z\uparrow]')\ ,$$

where S,X,Y,Z are the orbital components and $\uparrow$ and $\downarrow$ the spin eigenfunctions (see subsections 3 and 5 of Appendix A; for $\mathbf{k}=0$, $b=c=0$). G is a parameter arising from the coupling, in III-V compounds, between the lower conduction band (of Γ_6 symmetry) and the second conduction band (of Γ_5 symmetry).[20] When the value $G=5\hbar^2/2m$ is used, (see the discussion in Appendix B 1), in agreement with spin-relaxation studies[21] and hot-electron photoemission polarization experiments,[6] the LMTO and Kane's-model values of ω differ by less than 7 meV for the largest kinetic energy used in the present work ($\varepsilon\approx 1$ eV),[22] which does not yield to significant differences in precession effects.

Two different ranges are to be considered for ω, in relation with the conduction band dispersion (see subsections 3 and 4 of Appendix B): (i) for $k<10^9\ \mathrm{m}^{-1}$, i.e., $\varepsilon<0.2$ eV, the energy dispersion is parabolic, so that $\omega(\mathbf{k})$ increases as k^3, i.e., as $\epsilon^{3/2}$,[23] and (ii) for $0.4<\varepsilon<2$ eV, the energy dispersion can be expressed, with a maximum error of 20 meV over the whole energy range, by a linear law, and $\omega(\mathbf{k})$ also follows a linear relation.

C. Precession of $\mathcal{S}$ around $\omega(\mathbf{k})$

The classical equation

$$\frac{d\mathcal{S}}{dt}=\boldsymbol{\omega}(\mathbf{k})\times\mathcal{S} \tag{11}$$

is applicable to the evolution of the statistical average of electrons with spin $\frac{1}{2}$. This equation is easily integrated in the case of a ballistic electron traveling at constant $\mathbf{k}$ in the bulk solid. For an electron undergoing thermalization in the bulk or gaining energy in the BBR, the situation becomes complicated as ω and $\mathcal{S}$ are functions of the position.

We now separately consider the two different regions in which coherent precession occurs. The major ideas of the model are summarized in the main text, the detailed calculations are presented in Appendix C. The geometry of the problem is schematized in Fig. 11.

1. Precession inside the bulk solid

The number $n(\mathbf{k})$ of ballistic electrons reaching the surface $z=0$, with a momentum $\mathbf{k}$ making an angle

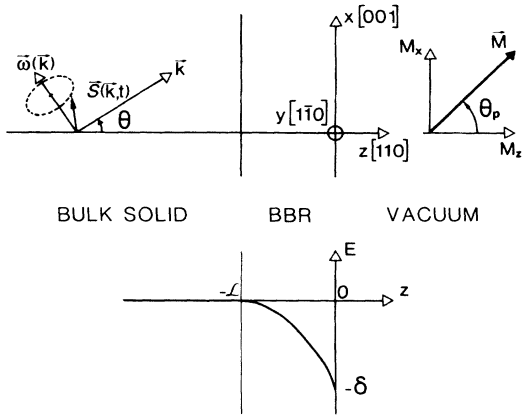

FIG. 11. Notations used in the calculations of Sec. III and Appendixes A and C.

θ ($0<\theta<\pi/2$) with the surface normal **z**, is given by

$$n(\mathbf{k})=\mathcal{n}(\mathbf{k})\int_{-\infty}^{0} e^{\alpha z}e^{z/(l\cos\theta)}\alpha\, dz\approx\mathcal{n}(\mathbf{k})\alpha l\cos\theta\ . \tag{12}$$

The first factor under the integral expresses the absorption with a characteristic depth α^{-1} ($\alpha^{-1}\approx 0.5-1$ μm in our excitation range) and the second one the probability for an electron excited at z ($z<0$) to reach the interface, l being the hot-electron mean free path ($l\approx 0.1$ μm); in the evaluation of (12) we take $\alpha l\ll 1$. The number $\mathcal{n}(\mathbf{k})$ of electrons excited from a given valence band with a momentum **k** is calculated in Appendix A [Eqs. (A3), (A18), and (A23)].

We consider a ballistic electron which suffers no collision after its promotion into the conduction band, i.e., keeps the same momentum **k**. The integration of Eq. (11) gives

$$\mathcal{S}(\mathbf{k},t)=(\mathcal{S}_0\cdot\boldsymbol{\omega})\frac{\boldsymbol{\omega}}{\omega^2}+\cos(\omega t)\left[\mathcal{S}_0-\mathcal{S}_0\cdot\boldsymbol{\omega}\frac{\boldsymbol{\omega}}{\omega^2}\right]-\sin(\omega t)\left[\mathcal{S}_0\times\frac{\boldsymbol{\omega}}{\omega}\right], \tag{13}$$

where $\mathcal{S}_0=\mathcal{S}(\mathbf{k},t=0)$ is the spin vector at promotion time $t=0$ as given in Appendix A [Eqs. (A4), (A17), and (A22)], and $\boldsymbol{\omega}$ stands for $\boldsymbol{\omega}(\mathbf{k})$, of modulus ω.

The spin contribution $\mathbf{S}(\mathbf{k})$ at $z=0$ of all the ballistic electrons with momentum **k** excited over the bulk crystal is obtained by an integral similar to Eq. (12):

$$n(\mathbf{k})\mathbf{S}(\mathbf{k})=\int_{-\infty}^{0} e^{\alpha z}e^{z/(l\cos\theta)}\mathcal{n}(\mathbf{k})\mathcal{S}(\mathbf{k},t)\alpha\, dz\ . \tag{14}$$

The time of precession t around $\boldsymbol{\omega}$ is $t=|z|/v\cos\theta$, for a velocity $v\cos\theta$ along z.

In the same approximation $\alpha l\leq 1$, Eq. (14) can easily be integrated into

$$\mathbf{S}(\mathbf{k})=\alpha l\cos\theta(\mathcal{S}_0\cdot\boldsymbol{\omega})\frac{\boldsymbol{\omega}}{\omega^2}+\frac{\alpha l\cos\theta}{1+(\omega l/v)^2}\left[\mathcal{S}_0-(\mathcal{S}_0\cdot\boldsymbol{\omega})\frac{\boldsymbol{\omega}}{\omega^2}\right]-\frac{\alpha l\cos\theta}{1+(\omega l/v)^2}\frac{\omega l}{v}\left[\mathcal{S}_0\times\frac{\boldsymbol{\omega}}{\omega}\right], \tag{15}$$

which expresses a "Hanle effect"[18] around the precession vector $\boldsymbol{\omega}$ during a characteristic time l/v.

The total number n of electrons (the total spin momentum $\mathbf{M}=n\mathbf{S}$) reaching $z=0$ is obtained by integration over **k** in the half-space $k_z>0$ of the $n(\mathbf{k})$ [$n(\mathbf{k})\mathbf{S}(\mathbf{k})$] contributions. The direction of the resulting mean spin **S** is then determined by symmetry considerations (see Appendix C 1): since the normal to the surface, parallel to [110] in our case, is taken as the **z** axis, we use for reference axes **x** parallel to [001] and **y** along [1$\bar{1}$0] (see Fig. 11). In this frame $\mathbf{h}(\mathbf{k})$ is given by

$$\mathbf{h}(\mathbf{k})=(2k_xk_yk_z,\ \tfrac{1}{2}k_z(k_z^2-k_y^2-2k_x^2),\ \tfrac{1}{2}k_y(k_y^2-k_z^2-2k_x^2))\ . \tag{16}$$

Neither component of $\mathcal{S}_0(\mathbf{k})$, along **k** or along **z**, gives any $\mathbf{S}_y$ contribution, so that the resulting spin **S** lies in the **x**-**z** plane and is rotated from the **z** direction by the angle $\theta_{\text{bulk}}=\arctan(S_x/S_z)$. Its modulus $|\mathbf{S}|=(S_x^2+S_z^2)^{1/2}$ is shorter than the result obtained for $\omega=0$, that is, in the absence of precession.

The precession and relaxation effects appear in **S** through a single parameter $\lambda=(\omega_0 l/v)$ (see Appendix C 2 a). In Figs. 12 and 13 we plot the calculated P_0 and θ_{bulk} versus λ for $\mathcal{S}_0\|\mathbf{z}$ (or $\mathcal{S}_0\|\mathbf{k}$). The measurement of θ_{bulk} or P_0 allows the estimation of λ and l since ω_0 and v are calculated from the band structure (see Appendix B 2). This requires the knowledge of the initial spin value $\mathcal{S}_0(\mathbf{k})$ and also the ability to separate the bulk contributions from those of the BBR in the measured precession angle and polarization.

Such calculations of the precession angle and of the maximum polarization are valid.

(i) For *ballistic* electrons excited from one of the three valence bands. The only part of the EDC without overlap between electrons promoted from different valence bands is the high-energy threshold, with electrons originating from the Γ_{8h} heavy-hole band. In this special case a value of $l(\varepsilon)$, where ε is the electron kinetic energy, should be deduced.

(ii) For *partly* or *completely thermalized* electrons. These electrons suffer relaxation in the bulk solid, which partly decorrelates their momentum and spin. For an electron submitted to collisions, each modification of **k** changes $\boldsymbol{\omega}(\mathbf{k})$, and the net effect of the bulk internal precession is a spin-relaxation mechanism,[2] as was already mentioned. However, precession may occur in the last step prior to emission into vacuum, a ballistic path with a characteristic distance of the order of the hot-electron mean free path, as determined for ballistic electrons from Γ_{8h} that would have the same kinetic energy at $z=0$.

2. *Precession in the band-bending region*

In this region of the sample ($-\mathcal{L}<z<0$), k_z and k are increasing with z. We assume a parabolic band bending, leading to an increase in kinetic energy

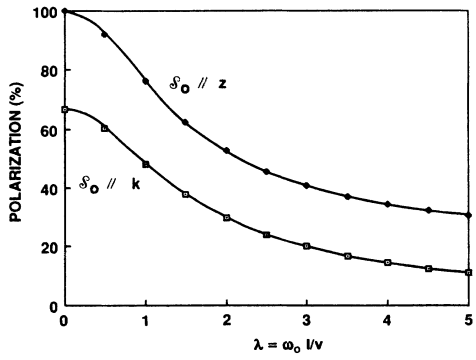

FIG. 12. Calculated polarization of ballistic electrons, after precession in the *bulk* solid, vs $\lambda=\omega_0 l/v$, for $\mathcal{S}_0\|\mathbf{k}$. In the case of $\mathcal{S}_0\|\mathbf{z}$, the data give the polarization for a spin fully polarized along **z** at creation.

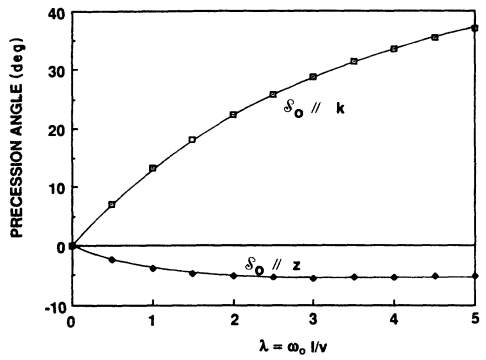

FIG. 13. Calculated precession angle of ballistic electrons, after precession in the *bulk* solid, vs $\lambda=\omega_0 l/v$, for $\mathcal{S}_0\|\mathbf{k}$ and $\mathcal{S}_0\|\mathbf{z}$.

$$\varepsilon(k)=\varepsilon(k_0)+[(z+\mathcal{L})/\mathcal{L}]^2\delta \ . \tag{17}$$

This expression introduces the momentum modulus k_0 when the electron enters the BBR at $z=-\mathcal{L}$ (see Fig. 11).

Then the time increment dt is related to dk_z by

$$dt=\frac{\hbar\mathcal{L}}{2[\delta(\varepsilon(k)-\varepsilon(k_0))]^{1/2}}dk_z \ . \tag{18}$$

In fact, for a given acceptor concentration, $\mathcal{L}$ and δ are related through Eq. (4).

For ballistic electrons, the exact procedure for determining the BB contribution to the precession angle consists of calculating the evolution of $\mathbf{S}(\mathbf{k})$ in the BBR, and integrating over all $\mathbf{k}$ directions. This leads to heavy numerical calculations. To simplify, we assume, and this will be justified *a posteriori*, that the band-bending precession is a rather small angle. Here we only recall the most important points of the calculation given in Appendix C 3.

(i) Due to the symmetry of the problem, precession takes place in the x-z plane.

(ii) For a given $\mathbf{k}_0$ in the bulk (with $k_{z0}>0$), precession in the BBR affects the spin $\mathbf{S}_b=\mathbf{S}(\mathbf{k}_0)$, entering the BBR after possible precession in the bulk, by

$$\begin{aligned}\Delta S_x(\mathbf{k}_0)&\approx S_{bz}\int_0^\tau\omega_y dt-S_{by}\int_0^\tau\omega_z dt \ ,\\ \Delta S_z(\mathbf{k}_0)&\approx S_{by}\int_0^\tau\omega_x dt-S_{bx}\int_0^\tau\omega_y dt \ ,\end{aligned} \tag{19}$$

where τ is the electron time of flight through the BBR. These expressions evidence that the observed net precession is determined by (i) the bulk precession, (ii) the kinetic energy at $z=-\mathcal{L}$, which gives the magnitude of the precession vector, and (iii) the precession time, also related to $\mathcal{L}$ and δ, i.e., to the doping level. The net spin momentum $\mathbf{M}=n\mathbf{S}$ after crossing the BBR is obtained by averaging over the directions allowing emission:

$$\begin{aligned}M_x&=\int n(\mathbf{k})(S_{bx}+\Delta S_x)\frac{d\Omega}{2\pi} \ ,\\ M_z&=\int n(\mathbf{k})(S_{bz}+\Delta S_z)\frac{d\Omega}{2\pi} \ .\end{aligned} \tag{20}$$

The total precession angle θ_p is equal to $\arctan(M_x/M_z)$. Two extreme cases are studied in Appendix C 3, depending on the value of $\mathbf{S}_b$.

(a) For an isotropic momentum distribution of electrons all carrying the same spin along z in the bulk ($\mathbf{S}_b=S_{bz}\mathbf{z}$), relations (19) simplify and become

$$\begin{aligned}\Delta S_x(\mathbf{k}_0)&\approx S_{bz}\int_0^\tau\omega_y dt \ ,\\ \Delta S_z(\mathbf{k}_0)&\approx 0 \ .\end{aligned} \tag{21}$$

This approximate expression of the resulting BB precession angle, $\Delta S_x(\mathbf{k}_0)/S_{bz}$, is the same as in Eq. (5), which was rigorously established in the case of thermalized electrons.

Because of the angular dependence of ω_y, the contribution to the BB precession of momenta making a small angle with the z axis is positive, whereas the contribution of momenta at large angles from z is negative, as can be seen in Fig. 14.

Figure 15 shows the calculated mean precession built up in the BBR versus the emitted electron energy, in the case of a thermalized electron distribution, for $\delta=0.3$ and 0.7 eV and $N_A=1.3\times10^{18}$ cm^{-3}. Note that negative precession angles are expected for smaller energies for $\delta=0.3$ eV: this comes from the fact that the isotropic distribution in the bulk (which would give a negative precession angle) is not modified much by the transport through the BBR, so that the contribution of momenta at large angles from z still dominates in the BBR.

Note that the calculated BB precession angles range between $-20°$ and $+20°$ for reasonable values of δ, as can be seen in Fig. 16. This justifies the "small-angle" approximation made in Eq. (19).

(b) In Appendix C 3 b we consider the additional precession experienced in the BBR by ballistic electrons promoted from Γ_{8h} and having already precessed in the bulk

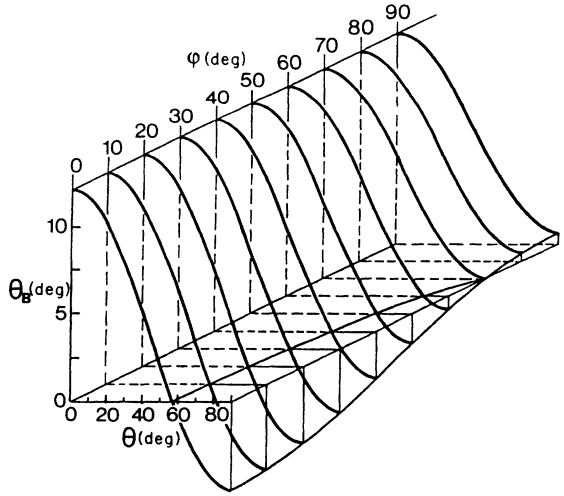

FIG. 14. Calculated BB precession θ_B for an electron with a spin along the direction z of the normal to the surface (i.e., along [110]) and a momentum orientation when entering the BBR defined by the angle θ and the azimuthal angle φ. The initial energy $\varepsilon(k_0)$ is equal to 0.4 eV and the BB energy $\delta=0.60$ eV.

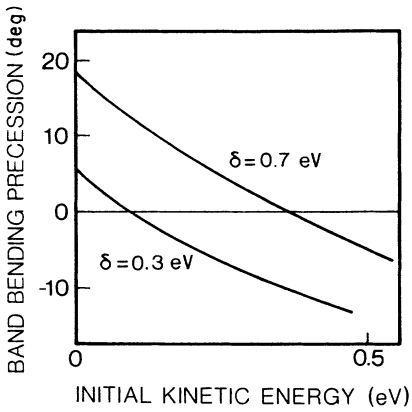

FIG. 15. Calculated BB precession for an isotropic distribution of electrons with a given kinetic energy $\varepsilon(k_0)$, and spins along z, when entering the BBR. The calculation is performed vs $\varepsilon(k_0)$ for two values of the BB energy δ.

crystal, which defines the value of $\mathbf{S}_b$. When the BB energy is not larger than the ballistic-electron energy, this coherent precession does not very significantly modify either the bulk precession angle or the bulk polarization value.

IV. DISCUSSION OF THE EXPERIMENTAL RESULTS

In this section we use the above models of spin precession and define a procedure to analyze the experimental $\theta_p(\varepsilon)$ curves. Then we discuss our data, and finally indicate the limits of application of our model.

In the spin-precession phenomenon, the important factors are the *magnitude of* $\omega(\mathbf{k})$ determined by G, the *BB energy* δ, the *shape of the momentum distribution,* and the *hot-electron mean free path* l for ballistic electrons. For G we use the value $5\hbar^2/2m$ already indicated in Sec. III B. The BB width can be calculated using Eq. (4) from the known doping level, once δ is given. We thus take δ and $l(\varepsilon)$ as parameters to be deduced from the experimental data. There should be consistency over their determinations from the different parts of the spectra and for different excitation energies.

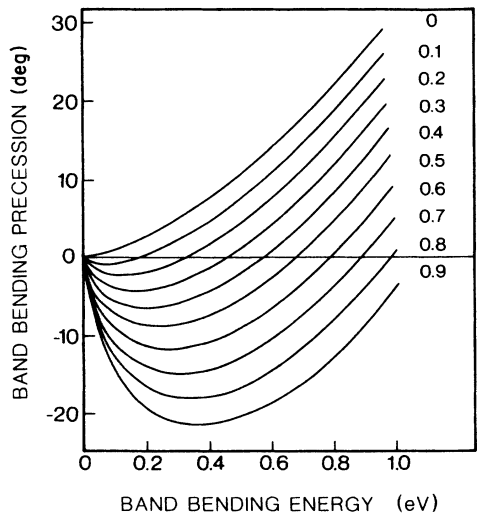

FIG. 16. Calculated BB precession for an isotropic distribution of electrons with a given energy $\varepsilon(k_0)$, and spins along z, when entering the BBR. The calculation is performed vs the BB energy δ for several values of $\varepsilon(k_0)$.

We successively consider the lowest-energy part of the precession spectrum, which allows an estimate of δ (Sec. IV A); the spin precession in the intermediate-energy range, leading to an independent determination of δ, and the possible effect of electrons relaxed in the L and X minima (Sec. IV B); the highest-energy part of the spectrum, leading to an estimation of the hot-electron mean free path l (Sec. IV C).

A. Lowest-energy range

The low-energy part is limited by the vacuum-level cutoff. Since it contains the dominant contribution to the photoemitted current,[7] it determines the overall polarization and, for a nonvanishing thermalized-electron polarization, the spin precession in the energy-integrated measurements. Because we only observe the part of the Γ peak merging above the vacuum level, we cannot unambiguously state that the electrons emitted at the lowest energy ("thermalized electrons") originate from electrons thermalized in the bulk solid, having possibly lost energy in the BBR. Nevertheless, we will assume that their polarization and precession angles are not significantly different from those of the truly thermalized electrons. This assumption may lead to an underestimate of θ_p. In the low-energy range, if the energy dispersion is taken as parabolic, by integration of Eq. (5) and use of Eq. (18) we find that θ_p is proportional to $\mathcal{L}\delta$, i.e., to $\delta^{3/2}N_A^{-1/2}$: then, underestimating θ_p would yield a too small value of δ.

On the low-temperature spectra for $h\nu=1.83$, 1.92, and 1.96 eV taken with an almost zero affinity (Fig. 9), the thermalized electrons have the same spin precession ($\approx 5°$), within the error bars, whatever $h\nu$. This fact confirms that for such electrons θ_p is built up in the BBR. From this value, using the calculation of the BB precession of Sec. III [Eqs. (21)] we deduce $\delta \approx 0.4$ eV. For $h\nu=2.18$ and 2.34 eV (Fig. 10), the sample is under positive electron affinity and the mean electron spin suffers a very large precession for ε close to zero, probably because of the selection at emission of electrons with momenta approximately normal to the crystal surface.[24,25]

In the spectra taken at 300 K for near-band-gap excitation ($h\nu=1.55$ eV) (Fig. 8), the measurement $\theta_p \approx 18°$ can only be interpreted by $\delta \approx 0.7$ eV. Such a variation of BB energy with temperature can be predicted in models where both donor- and acceptor-surface states are present.[26] In the other 300-K spectra in Fig. 8 the "thermalized" electrons suffer a spin precession, which becomes more negative when $h\nu$ increases from 1.55 to 1.92 eV. In fact, the affinity is only slightly negative, so that a part of the signal arises from more energetic electrons, which lost some energy in the BBR and overlap with the true thermalized electrons.

B. Intermediate-energy range

Such a distinct range exists for sufficient photon energies ($h\nu \geq 1.96$ eV) and we discuss it on the 110-K data (Figs. 9 and 10). For $h\nu = 1.96$ eV the precession angle θ_p is positive, but smaller than for $h\nu = 1.83$ or 1.92 eV. For $h\nu = 2.18$, 2.34, and 2.60 eV, negative θ_p's are observed. In fact, the change in sign of precession is not correlated to the threshold for emission of electrons from the L ($\varepsilon > 0.3$ eV) or X ($\varepsilon > 0.45$ eV) minima,[27] or for excitation from the spin-orbit-split Γ_7 valence band. We observe it at an energy ≈ 0.3 eV lower than that of the ballistic electrons excited from Γ_{8h}, whatever $h\nu$.

As discussed in Sec. III C 2, negative precession angles come from off-normal $\mathbf{k}$, i.e., they are built up when a quasi-isotropic momentum distribution enters the BBR. The theoretical curves in Fig. 16 represent the BBR precession angle versus δ, for an isotropic momentum distribution entering the BBR with spins along z. These curves set an upper limit to the value of δ which permits observation of a negative spin precession in this energy region: the measurement $\theta_p = -9°$ for $\varepsilon = 0.48$ eV, $h\nu = 2.60$ eV implies $\delta < 0.50$ eV at low temperature. By comparing the experimental and calculated precessions, we deduce that the electron distribution becomes isotropic after an energy loss of about 0.3–0.4 eV below the high energy threshold.

In Fig. 10 the low-energy zeros of the $\theta_p(\varepsilon)$ curves seem to occur at the same kinetic energy $\varepsilon \approx 70$ meV for the three excitation energies 2.18, 2.34, and 2.60 eV. Since the observed structures in the EDC's are downshifted by more than 100 meV because of energy loss in the BBR,[7,16] the bulk energy for which $\theta_p = 0°$ should be of the order of 0.20 eV. According to the theoretical curves in Fig. 16, this should correspond to a BB energy of the order of 0.35 eV, a value not far from the estimate made in Sec. IV A.

The very large negative θ_p for $h\nu = 2.18$ and 2.34 eV cannot be explained by our parameters, which fit the low-energy range. Since the electrons excited from the Γ_7 valence band are responsible for the observed negative polarization,[6] their spin precession has to be taken into account. This contribution, evaluated in the ballistic-electron model presented in Appendix C 2 a, was considered; however, it gives negative precessions still too small by a factor of ≈ 2.

Electrons accumulated in the L minima, and having suffered energy relaxation in the BBR prior to emission, could contribute to θ_p in this energy range. Since the conduction band is also spin-split in the vicinity of the L minima,[28] we expect a spin precession related to this spin splitting. In order to calculate the corresponding precession vector ω_L, after Ref. 28, we have used the $\mathbf{k}\cdot\mathbf{p}$ description of the bands around the L point and then added the spin-orbit interaction as a perturbation. It can be shown that ω_L is proportional to $\mathbf{k}\times\hat{\mathbf{L}}$, where $\hat{\mathbf{L}}$ is the unit vector along the considered L direction. Four $\langle 111 \rangle$ directions have a component on the (110) normal to the surface. For these directions the gain of momentum in the BBR is such that it results in a nonzero transverse spin component. Electrons having a small impulsion in the four L valleys belonging to the (110) plane also suffer precession. The in-plane and out-of-plane masses are unequal; the corresponding contributions to the precession angle differ in value and sign. Then the net spin precession for electrons emitted from L has a complicated variation.[29] Besides, the measurements on (100) GaAs (Ref. 6) showed that electrons emitted after energy relaxation in the L minima are depolarized through the spin-relaxation mechanism associated with the L-valley spin splitting: such electrons will not affect the observed spin precession.

Electrons can also be accumulated in the X minima, for $h\nu \geq 2.18$ eV. The spin precession in the X minima differs greatly from that in the L ones, since, to first order in the $\mathbf{k}\cdot\mathbf{p}$ perturbation, for X taken as [001], ω_X is now proportional to $(k_x, -k_y, 0)$. The deduced precessions for the different X valleys do not average to zero. Because the X structure is weak in the EDC's, as can be seen in Fig. 5, its contribution to the spin precession will not drastically affect the overall shape of the spectrum. Yet we expect an enhancement of the negative precessions, as will be discussed in a forthcoming paper.[29]

An explanation for the overly small calculated precession angles could be a reduction of the doping level near the surface, leading to an increase in the BB width $\mathcal{L}$, after heating the sample at ≈ 850 K in the cleaning procedure. A larger $\mathcal{L}$ could also better explain the blurring of the hot-electron structures in the EDC's (see Sec. II C). The value of the BB energy deduced from the precession-angle measurement in the lowest-energy range would be somewhat reduced, yet in our experiment this determination is not the most reliable one (see Sec. IV A). In fact, the estimation of δ from the zero of the $\theta_p(\varepsilon)$ curves, in the intermediate-energy range, given by Eq. (C19), which is independent of $\mathcal{L}$, would not be modified. In the limit of the experimental uncertainties, the determinations of δ in these two ranges would remain consistent.

From this discussion on the intermediate-energy-range results, we can conclude that the steep decrease in θ_p reported in energy-integrated experiments for $h\nu > 1.8$ eV (Ref. 9) is not due to side-valley effects but rather to the contribution of an isotropized nonthermalized-electron distribution crossing the BBR. This contribution becomes important because, for these excitation energies, the thermalized electrons are strongly depolarized.

C. Highest-energy part of the spectrum

The low-temperature results on ballistic electrons provide two data, the precession angle and the spin polarization. As explained in Sec. III C 2, the *bulk* contributions to these parameters are both determined by $\lambda = \omega_0 l / v$. To analyze these data, we assume that the only process reducing the bulk polarization is the precession effect considered here: this is supported by the study on (100) GaAs;[6] we neglect the effect of the BBR as mentioned in Sec. III C 2, because for our photon energies the kinetic energy at excitation is of the order, or larger than, the BB energy (0.4 eV) determined in Sec. IV A.

The measured values of θ_p and P_0 at a given kinetic energy give two independent determinations of λ, which should be consistent if only ballistic electrons were emitted. Practically, for $h\nu \leq 2.34$ eV we deduce from P_0 a value of λ approximately 2 times larger than that obtained from θ_p. For $h\nu = 2.60$ eV the λ deduced from P_0 is even 5 times larger than its determination from θ_p, but in this latter case the measurement at the highest kinetic energy is performed as far as 0.18 eV from the promotion energy, so that the ballistic-electron contribution can no longer be isolated and we observe electrons having lost some energy. For the other $h\nu$'s the measured extreme kinetic energies are 40–80 meV below the high-energy threshold: measurements at the threshold were impossible because of the extreme weakness of the emitted currents; indeed, much smaller than those emitted from (100) GaAs surfaces in the same conditions. This smaller yield could be attributed to the poor transmission coefficient of the (110) surface, as pointed out in the calculation of Burt and Inkson.[30] In such a situation, the exact prediction of θ_p and P_0 would require information on the momentum, energy, and spin-relaxation mechanisms.

Qualitatively, the anisotropy of the momentum distribution should be reduced by this low transmission: if purely ballistic electrons can no longer be isolated, the contribution of the BBR to the precession angle should decrease and even become negative for a totally isotropic distribution. Then, the observed θ_p would be smaller than expected for ballistic electrons, and would correspond to underestimated values of λ. Conversely, the admixture of nonballistic electrons leads to a further polarization reduction, so that the λ values determined from P_0 appear as upper limits. We can then conclude that the true λ values are bounded between the two estimations, from θ_p and P_0. However, polarized hot luminescence[3] and polarized hot photoemission results[6] show that the decrease of polarization is not drastic on the first 50 meV below the high-energy threshold. Thus we consider the λ value deduced from P_0 as more reliable, take the observed P_0 as the bulk value, and for each exciting photon energy we determine $\lambda = \omega_0 l / v$ and, consequently, the expected bulk precession θ_{bulk}. From λ we deduce $l(\varepsilon)$ at excitation from Γ_{8h} (see Appendix B).

As can be seen in Table II, l decreases from 150 nm ($\varepsilon = 0.30$ eV) to 110 nm ($\varepsilon = 0.91$ eV). These values are consistent with the determinations on (100) GaAs ($p \approx 10^{19}$ cm^{-3}) in which $l \approx 75$ nm in this energy range:[31] a higher doping level shortens l in this concentration range where electron-hole collisions are the dominant energy-relaxation mechanism.[32,33]

TABLE II. Hot-electron mean free path deduced from the highest-energy part of the spectrum (Sec. IV C).

	ε (eV)					
	0.30	0.37	0.40	0.58	0.70	0.91
λ	2	2.2	2.5	3.2	3.6	4.6
l (nm)	150	130	140	120	110	110

The spectra at 300 K evidence a very important depolarization in the hot-electron region. This prevents any quantitative analysis and suggests the presence of an additional spin-relaxation mechanism.

V. CONCLUSION

In the present paper we have thoroughly studied spin-precession phenomena versus the electron kinetic energy in a noncentrosymmetric semiconductor. This analysis completes the study of spin-polarized photoemission and proposes a more accurate estimation of the hot-electron mean free path, taking into account the conduction-band nonparabolicity. From Kane's $\mathbf{k}\cdot\mathbf{p}$ band model we have also derived a density-matrix formalism equivalent to that used in D'ymnikov-D'yakonov-Perel' calculations. The link between the two descriptions is clearly established.

However, the originality of this paper stands in the measurement of the angle between the normal to the semiconductor surface and the spin vector at emission *as a function of kinetic energy* under excitation by photons of a given energy $h\nu$. This technique gives access to band-bending properties, to the magnitude of the internal magnetic field, and provides a picture of the evolution of the electron-distribution anisotropy. In the high-kinetic-energy range, the ballistic electrons, with an anisotropic spin and momentum distribution, suffer spin precession mainly in the bulk solid. In the lower-energy range, the spin precession essentially builds up in the band-bending region (BBR): (i) the electrons *thermalized* in the bulk solid all gain the same momentum in the BBR; this highly anisotropic momentum distribution leads to a spin precession of the *same* sign as that of the hot ballistic electrons; (ii) in the intermediate-energy range, the electrons enter the BBR with an isotropic momentum distribution which, for sufficient initial kinetic energy, yields to a spin precession of the *opposite* sign.

Energy-resolved measurements are particularly suited to clarify spin-polarized photoemitted-electron-beam properties. For example, in energy-integrated experiments, both polarization and precession curves show a steep decrease for $h\nu \geq 1.8$ eV. In the study of the energy-resolved polarization data,[6] it was emphasized that this decrease is not due to electrons excited from the spin-orbit-split valence band, but rather to the contribution of electrons excited from the light-hole band, which becomes parallel to the heavy-hole one in this energy range. In the present energy-resolved precession experiments, we establish that the precession decrease is not due, as was previously supposed, to the contribution of electrons relaxed in the L valleys, but rather to that of an isotropic electron distribution crossing the band-bending region.

ACKNOWLEDGMENTS

We thank G. Lampel for his constant interest in this work, G. Fishman for fruitful discussions, P. Bréchet, R. Houdré, and D. Paget for a careful reading of the

manuscript and J.-P. Hermann for help in the calculations. H. R. would like to thank the Laboratoire de Physique de la Matière Condensée for providing the pleasant and exciting working atmosphere. He furthermore thanks Professor M. Campagna for his interest and support for this work. He gratefully acknowledges the efficient support from Arbeitsgemeinschaft der Grossforschungseinrichtungen (Bonn, West Germany) and Centre National de la Recherche Scientifique (Paris, France) which made his stay at Ecole Polytechnique possible. H.-J.D. is a member of the Direction des Recherches, Etudes et Techniques de la Délégation Générale pour l'Armement (France). Laboratoire de Physique de la Matière Condensée is "Unité de Recherche Associée au Centre National de la Recherche Scientifique, France."

APPENDIX A: DENSITY MATRIX AND MEAN SPIN AT CREATION

This appendix does not take into account the effects related to the spatial inhomogeneity of light absorption, which are discussed in the main text [Eqs. (12), (14), and (15)].

1. Density matrix

For excitation by a photon of given energy $h\nu$, which causes transitions between valence states $|v_j\rangle$ and conduction states $|c_l\rangle$, the conduction electron density operator $\underline{\rho}$ is deduced by application of the light dipolar operator $\underline{\mathbf{d}}$ on the initial valence states:

$$\underline{\rho}=\sum{}'\,\underline{\mathbf{d}}\,|v_j\rangle\langle v_j|\,\underline{\mathbf{d}}^{\dagger} \tag{A1}$$

where $\sum'$ expresses that the sum is restricted to valence states compatible with the conservation of momentum $\mathbf{k}$ and energy. Note that $\underline{\rho}$ is not a true density matrix since it is not normalized to unity. We assume that the energy bands are spherical and consider the conduction band as doubly spin-degenerate [we neglect the spin splitting related to $\omega(\mathbf{k})$]. Consequently the density operator reduces to a diagonal set of 2×2 matrices, each of them referring to a $\mathbf{k}$ direction at a given conduction energy. We want to show that, in a $\mathbf{k}\cdot\underline{\mathbf{p}}$ perturbation description of the valence and conduction states, the average spin vector of the conduction electrons, at excitation from any valence band, is the sum of two components, one parallel to the light propagation direction $\mathbf{z}$, and the second one along the electron momentum $\mathbf{k}$, of modulus k.

2. D'ymnikov, D'yakonov, and Perel' formalism

D'ymnikov, D'yakonov and Perel'[8] (DDP) calculate the interband radiative transitions in GaAs using the $k\approx0$ conduction states. A possible conduction basis is $|c_l\rangle=|[iS\uparrow]'\rangle$, $|[iS\downarrow]'\rangle$, i.e., spin eigenfunctions along the momentum direction. For excitation by circularly polarized light, these authors derive the electron density operator at the instant of excitation into the conduction band. The operator is the direct sum of all the $\underline{\rho}(\mathbf{k})$ operators, each one concerning the electrons created with a given momentum $\mathbf{k}$, for the different $\mathbf{k}$ satisfying energy conservation. Its expression in DDP's paper is

$$\underline{\rho}=\rho(k)\left[\left[1-\alpha_0\frac{3(\mathbf{n}\cdot\boldsymbol{\nu})^2-1}{4}\right]\underline{1}+2s_0\underline{\boldsymbol{\sigma}}\cdot\mathbf{n}+\beta_0\frac{3(\underline{\boldsymbol{\sigma}}\cdot\boldsymbol{\nu})(\mathbf{n}\cdot\boldsymbol{\nu})-\underline{\boldsymbol{\sigma}}\cdot\mathbf{n}}{2}\right] \tag{A2}$$

where $\underline{1}$ is the 2×2 unit matrix, and $\underline{\boldsymbol{\sigma}}$ are the 2×2 Pauli matrices. The unit vectors along the direction of the photon angular momentum (along the $\mathbf{k}$ momentum direction) are $\mathbf{n}(\boldsymbol{\nu})$. For σ^+ (σ^-) excitation, $\mathbf{n}$ is parallel (antiparallel) to the light propagation direction. The following calculations are performed for σ^- light excitation, for which $\mathbf{n}$ is the outgoing normal to the crystal. In the notations of the present paper we take $\mathbf{n}$ as $\mathbf{z}$ axis, and label $\boldsymbol{\nu}$ as $\mathbf{z}'$, to ensure coherency with Kane's notations (see Sec. 3 of this Appendix). Using $\underline{\rho}$ we calculate the average number of excited electrons $n(\mathbf{k})$ and the average spin vector $\mathcal{S}_0(\mathbf{k})$:

$$n(\mathbf{k})=\mathrm{Tr}\underline{\rho}=2\rho(k)\left[1-\alpha_0\frac{3(\mathbf{z}\cdot\mathbf{z}')^2-1}{4}\right], \tag{A3}$$

$$n(\mathbf{k})\mathcal{S}_0(\mathbf{k})=\mathrm{Tr}(\underline{\rho}\underline{\boldsymbol{\sigma}}/2)=2\rho(k)[(s_0-\tfrac{1}{4}\beta_0)\mathbf{z}+\tfrac{3}{4}\beta_0(\mathbf{z}\cdot\mathbf{z}')\mathbf{z}']\,. \tag{A4}$$

The parameters α_0, s_0, and β_0, characteristic of the initial valence band, are then easily interpreted: α_0 appears in the trace of $\underline{\rho}$ and is representative of the anisotropy of the electron number at creation; the angular averaged spin vector $\int n(\mathbf{k})\mathcal{S}_0(\mathbf{k})(d\Omega/4\pi)/\int n(\mathbf{k})(d\Omega/4\pi)$ is $s_0\mathbf{z}$ and β_0, which gives the spin component along the wave vector, and reflects the anisotropy of the initial spin distribution.

3. Starting from Kane's model

On the other hand, the upper valence- and lower conduction-band wave functions for $k\neq0$ are conveniently described by Kane's model,[1] using first-order $\mathbf{k}\cdot\underline{\mathbf{p}}$ perturbation theory. This leads to the two secular equations

$$E'=0\,, \tag{A5}$$

$$E'(E'-E_G)(E'+\Delta)-k^2P^2(E'+2\Delta/3)=0\,, \tag{A6}$$

where $E'(k)=E(k)-(\hbar^2/2m)k^2$. The energy origin is taken at the top of the valence band, E_G is the band-gap energy, Δ the valence-band spin-orbit splitting, m the free-electron mass, and $iPm/\hbar$ the momentum matrix element between valence- and conduction-band states. The doubly degenerate wave functions are given by

$$\phi_{h+}=|[(X+iY)\uparrow/\sqrt{2}]'\rangle\,,\qquad \phi_{h-}=|[(X-iY)\downarrow/\sqrt{2}]'\rangle\,, \tag{A7}$$

$$\phi_{i+}=a_i|[iS\uparrow]'\rangle+b_i|[-(X+iY)\downarrow/\sqrt{2})']\rangle+c_i|[Z\uparrow]'\rangle\,, \tag{A8}$$

$$\phi_{i-}=a_i|[iS\downarrow]'\rangle+b_i|[(X-iY)\uparrow/\sqrt{2}]'\rangle+c_i|[Z\downarrow]'\rangle\,,$$

with

$$a_i = kP(E_i' + 2\Delta/3)/N \ ,$$
$$b_i = (\sqrt{2}\Delta/3)(E_i' - E_G)/N \ , \quad \text{(A9)}$$
$$c_i = (E_i' - E_G)(E_i' + 2\Delta/3)/N \ .$$

The index h refers to the heavy-hole band obtained from Eq. (A5), the index i to the conduction ($i=6$), light-hole ($i=8$), and spin-orbit-split ($i=7$) bands, given by Eq. (A6). The primes denote that the wave functions are rotated in the $\mathbf{k}$ direction, with $\mathbf{k}$ taken as the $\mathbf{z}'$ axis ("local basis"); N is the normalization factor, so that

$$a_i^2 + b_i^2 + c_i^2 = 1 \ . \quad \text{(A10)}$$

The conduction eigenstates $|c_i\rangle = \phi_{6+}, \phi_{6-}$ can no longer be taken as pure spin states since b_i and c_i are different from zero. The application of a spin operator $\underline{\sigma}_i (i = x', y', z')$ on ϕ_{6+} (ϕ_{6-}) gives a state out of the subspace generated by ϕ_{6+} and ϕ_{6-}. The basis used for conduction states has to be extended to include such states, and we choose the basis $\{|c_l\rangle, |c_\ell\rangle\}$, with $\langle c_l | c_\ell \rangle = 0$. The calculation of spin mean values does not involve $|c_\ell\rangle$ states. Indeed each mean component is given by a trace such as

$$\mathrm{Tr}(\underline{\rho}\underline{\sigma}_i) = \sum{}' \langle c_l | \underline{\mathbf{d}} | v_j \rangle \langle v_j | \underline{\mathbf{d}}^\dagger \underline{\sigma}_i | c_l \rangle + \sum \langle c_\ell | \underline{\mathbf{d}} | v_j \rangle \langle v_j | \underline{\mathbf{d}}^\dagger \underline{\sigma}_i | c_\ell \rangle \ . \quad \text{(A11)}$$

The $|c_\ell\rangle$ states cannot be reached by light excitation from the $|v_j\rangle$ states contributing to $\sum'$, since these valence states are coupled to the $|c_l\rangle$ only, i.e., $\langle c_\ell | \underline{\mathbf{d}} | v_j \rangle = 0$. Then $\mathrm{Tr}(\underline{\rho}\underline{\sigma}_i)$ is restricted to its partial trace on $|c_l\rangle$ states; this is formally equivalent to projecting the Pauli operators $\underline{\sigma}_i$ on the (ϕ_{6+}, ϕ_{6-}) subspace into new operators $\underline{\Sigma}_i$:

$$\underline{\Sigma}_{x'} = (1 - b_6^2)\underline{\sigma}_{x'} \ ,$$
$$\underline{\Sigma}_{y'} = (1 - b_6^2)\underline{\sigma}_{y'} \ , \quad \text{(A12)}$$
$$\underline{\Sigma}_{z'} = (1 - 2b_6^2)\underline{\sigma}_{x'} \ ,$$

where the prime components are referred to the local basis. Now the value of b_6 can be estimated. Its definition is

$$b_6 = (\sqrt{2}\Delta/3)(E_6' - E_G)/N \ ,$$

with N given by

$$N = [(kP)^2(E_6' + 2\Delta/3)^2 + 2(\Delta/3)^2(E_6' - E_G)^2 + (E_6' - E_G)^2(E_6' + 2\Delta/3)^2]^{1/2} \ . \quad \text{(A13)}$$

Since E_6' satisfies the secular equation, b_6 is also equal to

$$b_6 = \sqrt{2}(\Delta/3)(E_6' - E_G)^{1/2}/N'$$

with

$$N' = [E_6'(E_6' + \Delta)(E_6' + 2\Delta/3) + 2(\Delta/3)^2(E_6' - E_G) + (E_6' - E_G)(E_6' + 2\Delta/3)^2]^{1/2} \ .$$

Observing that $E_6' - E_G \geq 0$ and that $\Delta > 0$, we deduce that

$$N' \geq E_6'(2E_6' - E_G)^{1/2}$$

and from the b_6 expression, we find

$$0 \leq b_6 \leq 0.16(\Delta/E_G) \quad (\approx 3 \times 10^{-2} \text{ for GaAs}) \ . \quad \text{(A14)}$$

Therefore the spin operators $\underline{\Sigma}_i$ will be taken as equal to the Pauli matrices $\underline{\sigma}_i$.

4. Correspondence between the two formalisms

From Kane's wave functions, we calculate $\underline{\rho}(\mathbf{k})$ and the mean spin $\mathcal{S}_0(\mathbf{k})$ for transitions from the different valence bands, with the aid of the following symmetry considerations, used in Ref. 1 to reduce the Hamiltonian and to establish the secular equations (A5) and (A6). The only non-zero momentum matrix elements are of the type

(a) $\langle S' | \underline{\mathbf{p}}_{x'} | S' \rangle$,

(b) $\langle S' | \underline{\mathbf{p}}_{x'} | X' \rangle$,

(c) $\langle X' | \underline{\mathbf{p}}_{x'} | X' \rangle$, $\langle X' | \underline{\mathbf{p}}_{x'} | Y' \rangle, \langle X' | \underline{\mathbf{p}}_{y'} | Z' \rangle$,

and similar terms obtained by permutations of the components.

From space symmetry[20] it is easy to establish the relations

(a) $\langle S' | \underline{\mathbf{p}}_{x'} | S' \rangle = 0$,

(b) $\langle S' | \underline{\mathbf{p}}_{x'} | X' \rangle = \langle S | \underline{\mathbf{p}}_x | X \rangle = imP/\hbar$.

Moreover, Dresselhaus[34] showed that all (c) terms vanish due to time-inversion symmetry.

For σ^- light excitation, the dipolar operator is $\underline{\mathbf{d}} = \underline{\mathbf{p}}_x + i\underline{\mathbf{p}}_y$. This definition of the dipolar operator is somewhat unusual. Indeed, the light propagation direction is usually taken as $\mathbf{z}$ axis, which implies $\underline{\mathbf{d}} = \underline{\mathbf{p}}_x + i\underline{\mathbf{p}}_y$ ($\underline{\mathbf{p}}_x - i\underline{\mathbf{p}}_y$) for σ^+ (σ^-) light. With our choice of axis orientation, convenient to calculate the spin precession, the light propagation direction is *opposite* to $\mathbf{z}$, therefore $\underline{\mathbf{d}} = \underline{\mathbf{p}}_x + i\underline{\mathbf{p}}_y$ for σ^- light. The angle between $\mathbf{z}$ and $\mathbf{k}$ is θ.

a. Transitions from the heavy-hole band

In the (ϕ_{6+}, ϕ_{6-}) local basis, $\underline{\rho}$ is given by

$$\underline{\rho}(\mathbf{k}) = \tfrac{1}{2}a_6^2(Pm/\hbar)^2 \begin{bmatrix} (\cos\theta - 1)^2 & 0 \\ 0 & (\cos\theta + 1)^2 \end{bmatrix} \quad \text{(A15)}$$

so that

$$\underline{\rho}(\mathbf{k}) = C\{[1 + (\mathbf{z}\cdot\mathbf{z}')^2]\underline{1} - 2(\mathbf{z}\cdot\mathbf{z}')(\underline{\sigma}\cdot\mathbf{z}')\} \quad \text{(A16)}$$

with $C = \frac{1}{2}a_6^2(Pm/\hbar)^2$. Then the mean spin $\mathcal{S}_0(\mathbf{k})$ lies along the direction of $\mathbf{k}$:

$$\mathcal{S}_0(\mathbf{k}) = -\mathbf{z}'\cos\theta/(1 + \cos^2\theta) \quad \text{(A17)}$$

and

$$\mathcal{n}(\mathbf{k}) = C(1 + \cos^2\theta) \ . \quad \text{(A18)}$$

b. Transitions from the light-hole band or spin-orbit-split band

The density matrix $\underline{\rho}_j(\mathbf{k})$ for the light-hole ($j=8$) or spin-orbit-split band ($j=7$) is

$$\underline{\rho}_j(\mathbf{k})=[A_j^2\sin^2\theta+B_j^2(1+\cos^2\theta)]\underline{1} +2B_j^2\cos\theta\,\underline{\sigma}'_z+2A_jB_j\sin\theta\,\underline{\sigma}'_x \tag{A19}$$

where

$$A_j=(Pm/\hbar)(a_6c_j+a_jc_6)$$

and (A20)

$$B_j=(Pm/\hbar)(a_6b_j-a_jb_6)/\sqrt{2}$$

are functions of k, i.e., of the kinetic energy. This transforms into

$$\underline{\rho}_j(\mathbf{k})=[(A_j^2+B_j^2)+(B_j^2-A_j^2)(\mathbf{z}\cdot\mathbf{z}')^2]\underline{1} -2A_jB_j(\underline{\sigma}\cdot\mathbf{z})+2B_j(A_j+B_j)(\mathbf{z}\cdot\mathbf{z}')(\underline{\sigma}\cdot\mathbf{z}')\ . \tag{A21}$$

In this case the mean spin momentum $\mathcal{n}(\mathbf{k})\mathcal{S}_0(\mathbf{k})$ is given by:

$$\mathcal{n}(\mathbf{k})\mathcal{S}_0(\mathbf{k})=-2B_j[A_j\mathbf{z}-(A_j+B_j)(\mathbf{z}\cdot\mathbf{z}')\mathbf{z}'] \tag{A22}$$

with

$$\mathcal{n}(\mathbf{k})=2[(A_j^2+B_j^2)+(B_j^2-A_j^2)(\mathbf{z}\cdot\mathbf{z}')^2]\ . \tag{A23}$$

Thus, in the general case, $\mathcal{n}(\mathbf{k})$ is a function of the kinetic energy through A_j and B_j, and also of the angle θ between the momentum and the normal to the surface; $\mathcal{S}_0(\mathbf{k})$ is made up of two components, one along $\mathbf{z}$, the other one along $\mathbf{z}'$ (i.e., along $\mathbf{k}$) and can be written

$$\mathcal{S}_0(\mathbf{k})=m_1\mathbf{z}+m_2\cos\theta\,\mathbf{z}' \tag{A24}$$

where m_1 and m_2 are functions of k alone.

c. Link between DDP and Kane formalisms

(i) Transitions from the heavy-hole band. By identification of formulas (A2) and (A17), we find

$$\alpha_0=-1,\quad \beta_0=1,\quad s_0=\tfrac{1}{4}\ . \tag{A25}$$

(ii) Transitions from the light-hole or spin-orbit-split bands. Comparing formulae (A2) and (A21) giving the density matrix $\underline{\rho}_j(\mathbf{k})$, we deduce

$$s_0=\frac{B_j^2-2A_jB_j}{2(2B_j^2+A_j^2)}\ ,$$
$$\alpha_0=2\frac{A_j^2-B_j^2}{2B_j^2+A_j^2}\ , \tag{A26}$$
$$\beta_0=2\frac{B_j^2+A_jB_j}{2B_j^2+A_j^2}\ .$$

Note that this identification of Kane's and DDP's formalisms is only possible when the effect of spin mixing is negligible in the conduction band, i.e., b_6^2 can be neglected [see Eqs. (A12)–(A14)]. If this condition was not verified, Kane's formalism should be used.

5. Small- and large-k limits

It is interesting to determine the limits of the electron distribution parameters near the Brillouin-zone center as well as for large k.

a. Small-k limit

From Eqs. (A9), we calculate the Kane coefficients for $k\to 0$ and obtain

$$a_6=1,\quad b_6=0,\quad c_6=0\ ,$$
$$a_7=0,\quad b_7=-(\tfrac{2}{3})^{1/2}\quad c_7=-(\tfrac{1}{3})^{1/2}\ , \tag{A27}$$
$$a_8=0,\quad b_8=-(\tfrac{1}{3})^{1/2},\quad c_8=-(\tfrac{2}{3})^{1/2}\ .$$

The corresponding α_0,β_0,s_0 are summarized in Table III.

b. Large-k limit

For large k (say $kP\gg E_G$), we see from Eq. (1.6) that two roots are diverging, namely $E'_6\sim kP$ and $E'_7\sim -kP$. As the product of the roots of the secular equation is $k^2P^2(2\Delta/3)$, we conclude that $E'_8\sim -2\Delta/3$ (this value is the distance between the light- and heavy-hole bands at large k, where they become parallel). Then $A_7=B_7=0$, $A_8=0$ and $B_8=Pm/2\hbar$. As the sum of the three roots is $E_G-\Delta$, then for the spin-orbit-split and conduction energies $E'_7+E'_6=E_G-\Delta/3$ and it is easy to show that

$$A_7\sim(Pm/2\hbar)(E_G+\Delta/3)/kP\ ,$$
$$B_7\sim-(Pm/\hbar)(\Delta/3)(E_G+2\Delta/3)/(kP)^2\ . \tag{A28}$$

It follows that $A_8/B_8\to 0$ and $B_7/A_7\to 0$ and, in fact, these ratios become rapidly negligible when $\mathbf{k}$ is at some distance of the zone center. Using these values, we deduce the electron distribution parameters which are presented in Table IV.

To summarize, for electrons excited from the heavy-hole band, $\mathcal{S}_0(\mathbf{k})$ remains parallel to $\mathbf{k}$ for any kinetic energy. For electrons excited from the light-hole band with a large kinetic energy, $\mathcal{S}_0(\mathbf{k})$ becomes parallel to $\mathbf{k}$, since this band gets a heavy-hole character. For an excitation from the spin-orbit-split band, at low kinetic energy $\mathcal{S}_0(\mathbf{k})$ is along $\mathbf{z}$, but it gains a component parallel to $\mathbf{k}$ with increasing kinetic energy.

TABLE III. Density-matrix parameters in the small-k limit.

Transition from	α_0	β_0	s_0
Γ_{8h}	-1	-1	$-\frac{1}{4}$
Γ_{8l}	-1	1	$-\frac{1}{4}$
Γ_7	0	0	$\frac{1}{2}$

TABLE IV. Density-matrix parameters in the large-k limit.

Transition from	α_0	β_0	s_0
Γ_{8h}	-1	-1	$-\frac{1}{4}$
Γ_{8l}	-1	1	$\frac{1}{4}$
Γ_7	2	0	0

APPENDIX B: CALCULATIONS OF $\omega(\mathbf{k})$ AND $\lambda=\omega_0 l/v$ IN KANE'S BAND MODEL

1. Various expressions of the precession vector $\omega(\mathbf{k})$

We first recall the correspondence between the different expressions of the precession vector found in the literature.

In Kane's paper[1] the precession effect occurs in second-order $\mathbf{k}\cdot\underline{\mathbf{p}}$ perturbation: the modulus of the matrix element of the cubic Hamiltonian between pure spin conduction states is written as

$$\tfrac{1}{2}\hbar\omega(\mathbf{k})=2\sqrt{2}(abG/k)h(\mathbf{k}) . \tag{B1}$$

G expresses the coupling of the conduction and valence bands through other bands of Γ_5 symmetry and arises from the lack of inversion symmetry in III-V compounds, $G=\mathcal{G}\hbar^2/2m$ where $\mathcal{G}$ is a dimensionless constant, and a and b are the conduction band wavefunction coefficients obtained by first order $\mathbf{k}\cdot\underline{\mathbf{p}}$ perturbation [Eq. (A9)] (the index 6 corresponding to the conduction band is omitted here).

D'yakonov and Perel'[2] introduce the dimensionless constant α such that

$$\hbar\omega(\mathbf{k})=[\alpha(2m^{*3}E_G)^{-1/2}]\kappa , \tag{B2}$$

where m^* is the conduction electron effective mass and $\kappa=\hbar^3\mathbf{h}(\mathbf{k})$. In this expression $\omega(\mathbf{k})$ increases as k^3, which is only true for small momenta, i.e., $kP\ll E_G$. To establish a correspondence between (B1) and (B2), we use the expressions of a and b to the lowest order in $\mathbf{k}\cdot\underline{\mathbf{p}}$ perturbation

$$a\approx 1-(kP/E_G)^2(3+4\eta+2\eta^2)/6(1+\eta)^2 , \tag{B3}$$

$$b\approx\sqrt{2}\eta[kP/3E_G(1+\eta)] \times[1-(kP/E_G)^2(9+10\eta+2\eta^2)/6(1+\eta)^2] , \tag{B4}$$

with $\eta=\Delta/E_G$, and obtain

$$\hbar\omega(\mathbf{k})=8G(P/E_G)[\eta/3(1+\eta)] \times[1-(kP/E_G)^2(6+7\eta+2\eta^2)/3(1+\eta)^2]\mathbf{h}(\mathbf{k}) . \tag{B5}$$

In GaAs $2mP^2/\hbar^2=28.8$ eV,[35] i.e., $P=1.7\times10^{-28}$ J m, $\Delta=0.34$ eV, and $E_G=1.52$ eV, so that the term in $(kP/E_G)^2$ remains small as long as $k<1$ nm^{-1}, so we drop it from now on. In (B5) enter P, and in (B2) m^*. These quantities are related in the three-band $\mathbf{k}\cdot\underline{\mathbf{p}}$ model:[1,36]

$$m/m^*=1+\tfrac{2}{3}\xi[(3+2\eta)/(1+\eta)] , \tag{B6}$$

where the dimensionless constant $\xi=P^2m/\hbar^2E_G$. Then the relation between α and $\mathcal{G}$ is given by:

$$\alpha=\frac{4\sqrt{2}}{3}\frac{\eta}{1+\eta}\left[\frac{m^*}{m}\right]^{3/2}\xi^{1/2}\mathcal{G} . \tag{B7}$$

Using the numerical values of η and ξ for GaAs, we get $\alpha=1.25\times10^{-2}\mathcal{G}$. The value quoted by Maruschchak *et al.*,[21] $\alpha=0.07\pm0.005$, corresponds to $\mathcal{G}=5.6\pm0.4$, and does not differ much from $\mathcal{G}\approx5$ used to analyze spin-polarized photoemission experiments.[6] It is consistent with the cyclotron resonance results of Zawadzki *et al.*[37] Note that Aronov *et al.* had previously measured $\alpha=0.06$,[38] i.e., $\mathcal{G}=4.8$.

Fishman and Lampel[23] write $\omega(\mathbf{k})$ as $\sqrt{2}(ab/\hbar k)B'\mathbf{h}(\mathbf{k})$, with $B'=4G$, and estimate $B'\approx10\hbar^2/2m$ in GaAs ($\mathcal{G}=2.5$). This value is too weak to provide reasonable parameters from hot electron photoemission experiments, in the case of emission from (100) or (110) surface. Therefore in the present paper we will use the value $\mathcal{G}=5$.

2. Principle of the calculation of λ

We use Kane's expression of $\omega(\mathbf{k})$. The conduction-band velocity $\mathbf{v}=(1/\hbar)\nabla_{\mathbf{k}}(\varepsilon)$ is deduced from the energy dispersion $\varepsilon(k)$, where ε is the kinetic energy, also obtained from second-order $\mathbf{k}\cdot\underline{\mathbf{p}}$ perturbation: As discussed in Ref. 36 the energy dispersion of the lower Γ_6 conduction band is strongly influenced by the interaction with the upper Γ_5 conduction band, not included in first-order perturbation. We calculate $\omega(\mathbf{k})$ and λ in the small-k ($kP\ll E_G$) and large-k limits, and perform analytical expansions in order to get a physical insight. Numerical results are then given for the real intermediate range.

3. Small-momentum limit ($kP\ll E_G$)

We use expansion (B5). For $\mathbf{k}$ along [110], $h(\mathbf{k})=\frac{1}{2}k^3$, so that

$$\hbar\omega_0\approx4G(P/E_G)[\eta/3(1+\eta)]k^3 . \tag{B8}$$

In this energy range the effective mass m^* is defined by the parabolic energy dispersion $\varepsilon=\hbar^2k^2/2m^*$, the velocity $\mathbf{v}$ is equal to $\hbar\mathbf{k}/m^*$. Then $\lambda=\omega_0 l/v$ is given by:

$$\lambda=l\varepsilon(8m^{*2}/3\hbar^4)G(P/E_G)[\eta/(1+\eta)] , \tag{B9}$$

which is conversely written as

$$\varepsilon\approx(\lambda/l)\mathcal{A} ,$$

with

$$\mathcal{A}=(3\hbar^4/8m^{*2})(E_G/GP)[(1+\eta)/\eta] . \tag{B10}$$

We replace the band parameters by their values in GaAs ($m^*/m=0.067$, the experimental value):

$$\hbar\omega_0=33k^3(1-0.84k^2)\ \text{meV} ,$$

where k is in nm^{-1} units.

$$\varepsilon = 2.1\times 10^{-8}\lambda/[l(\mathrm{m})]\ \mathrm{eV} \tag{B11}$$

4. Large-momentum limit ($kP \gg E_G$)

As discussed in subsections 3 and 4 of Appendix A, in this limit Kane's third-degree secular equation provides a conduction-band eigenenergy E'_6 of the order of kP above Γ_8. By expansion around this value we find

$$E'_6 \approx kP + (3E_G - \Delta)/6 \ . \tag{B12}$$

so that the velocity v is a constant: $v \approx P/\hbar$. In the calculation of the precession vector $\omega(\mathbf{k})$ enter the limits of a and b:

$$a \approx (1/\sqrt{2})[1 + (3E_G + \Delta)/12kP] \ ,$$
$$b \approx (\Delta/3kP)[1 - (9E_G + 7\Delta)/12kP] \ . \tag{B13}$$

To this order of approximation ω_0 is a linear function of k

$$\hbar\omega_0 \approx (2\Delta G/3P)[k - (E_G + \Delta)/2P] \ . \tag{B14}$$

Using the expressions of ω_0 and v, we deduce λ:

$$\lambda = l(2\Delta G/3P^2)[k - (E_G + \Delta)/2P] \ . \tag{B15}$$

We only consider the Γ valley in the lower conduction band. Because of the large free-electron mass, we can assimilate $\varepsilon = E'_6 - E_G + (\hbar^2 k^2/2m)$ to $E'_6 - E_G$, i.e., $\varepsilon \approx kP - (3E_G + \Delta)/6$. Then there is again a linear relation between ϵ and λ:

$$\varepsilon = (\lambda/l)(3P^3/2\Delta G) + \Delta/3 \ , \tag{B16}$$

which allows us to deduce $l(\varepsilon)$ from the $\varepsilon(\lambda)$ values. For the GaAs band parameters (B9)–(B16) give (k is expressed in nm^{-1} units)

$$\begin{aligned} &E'_6 \approx 1.06k + 0.70\ \mathrm{eV} \ , \\ &v = 1.6\times 10^6\ \mathrm{m/s} \ , \\ &\varepsilon = 1.06(k - 0.77)\ \mathrm{eV} \ , \\ &\hbar\omega_0 = 41(k - 0.88)\ \mathrm{meV} \ , \\ &\lambda = 3.9(k - 0.88)\times 10^7 [l\ (\mathrm{m})] \ , \\ &\varepsilon = 2.7\times 10^{-8}\lambda/[l\ (\mathrm{m})] + 0.11\ \mathrm{eV} \ . \end{aligned} \tag{B17}$$

5. Numerical estimations

In the domain ($1 \le k \le 3\ \mathrm{nm}^{-1}$, i.e., $0.4 \le \varepsilon \le 2.1$ eV), which corresponds to our experimental situation, the numerical resolution of the third degree secular equation evidences almost linear variations, which can be approximated by:

$$\varepsilon \approx 0.824(k - 0.47)\ \mathrm{eV}, \quad \text{accurate within 15 meV in this range} \ , \tag{B18}$$

$$\hbar\omega_0 = 30.8(k - 0.49)\ \mathrm{meV} \ , \tag{B19}$$

$$v = 1.23\times 10^6\ \mathrm{m/s} \ .$$

We deduce

$$\lambda = 3.8(k - 0.49)10^7 [l\ (\mathrm{m})]$$
$$\varepsilon = 2.17\times 10^{-8}\lambda/[l\ (\mathrm{m})] + 0.01\ \mathrm{eV} \ ,$$

i.e.,

$$\varepsilon \approx 2.17\times 10^{-8}\lambda/[l\ (\mathrm{m})]\ \mathrm{eV} \ . \tag{B20}$$

In our physical situation the hot electron mean free path l is a function of ε. The experience yields values of λ, and we deduce $l(\varepsilon)$.

Notice that the relations $\varepsilon(\lambda)$ obtained in (B11), (B17), or (B20), that is, in all k ranges, give very similar slopes.

APPENDIX C: EVALUATION OF THE SPIN PRECESSION

1. Symmetry properties of the spin momentum components

The evolution of a spin $\mathcal{S}(\mathbf{k})$ submitted to a precession vector $\omega(\mathbf{k})$ is governed by the equation

$$\frac{d\mathcal{S}(\mathbf{k})}{dt} = \omega(\mathbf{k}) \times \mathcal{S}(\mathbf{k}) \ . \tag{C1}$$

Starting from this general expression, the direction of the spin vector at emission, averaged over all $\mathbf{k}$ directions, can be simply predicted from symmetry arguments.

a. (110) face

We use the axes defined in Sec. III C 1 and Fig. 11 and consider the transformation $(k_x, k_y, k_z) \to (k_x, -k_y, k_z)$. The precession vector $(\omega_x, \omega_y, \omega_z)$ is transformed into $(-\omega_x, \omega_y, -\omega_z)$ [see Eq. (16)], and the spin vector $\mathcal{S}^+ = (\mathcal{S}_x^+, \mathcal{S}_y^+, \mathcal{S}_z^+)$ becomes $\mathcal{S}^- = (\mathcal{S}_x^-, \mathcal{S}_y^-, \mathcal{S}_z^-)$. The following set of equations is deduced:

$$\begin{aligned} \frac{d(\mathcal{S}_x^+ - \mathcal{S}_x^-)}{dt} &= \omega_y(\mathcal{S}_z^+ - \mathcal{S}_z^-) - \omega_z(\mathcal{S}_y^+ + \mathcal{S}_y^-) \ , \\ \frac{d(\mathcal{S}_y^+ + \mathcal{S}_y^-)}{dt} &= \omega_z(\mathcal{S}_x^+ - \mathcal{S}_x^-) - \omega_x(\mathcal{S}_z^+ - \mathcal{S}_z^-) \ , \\ \frac{d(\mathcal{S}_z^+ - \mathcal{S}_z^-)}{dt} &= \omega_x(\mathcal{S}_y^+ + \mathcal{S}_y^-) - \omega_y(\mathcal{S}_x^+ - \mathcal{S}_x^-) \ , \end{aligned} \tag{C2}$$

From Eq. (A4), at excitation into the conduction band,

$$\mathcal{S}_x^+ - \mathcal{S}_x^- = \mathcal{S}_y^+ + \mathcal{S}_y^- = \mathcal{S}_z^+ - \mathcal{S}_z^- = 0 \ . \tag{C3}$$

The same condition is obviously satisfied for a spin distribution with $\mathcal{S}$ along z. Since zero is a solution of system (C2) with this initial condition, we deduce that condition (C3) remains valid during the whole evolution. Moreover, $\kappa(k_x, k_y, k_z) = \kappa(k_x, -k_y, k_z)$ [see Eq. (A3)], so that the resulting spin momentum after precession carries no y momentum, i.e., it lies in the x-z plane.

b. (100) face

The same analysis is carried out, taking the cubic crystallographic axes as the reference frame and making the transformation $(\kappa_x, \kappa_y, \kappa_z) \to (-\kappa_x, -\kappa_y, \kappa_z)$, which

transforms $(\omega_x,\omega_y,\omega_z)$ into $(-\omega_x,-\omega_y,\omega_z)$ [see Eq. (8)]. We find that $\mathcal{S}_x^+ + \mathcal{S}_x^- = \mathcal{S}_y^+ + \mathcal{S}_y^- = \mathcal{S}_z^+ - \mathcal{S}_z^-$ remains equal to zero during the precession, so that the resulting spin remains along z.

2. Bulk precession

We consider all electrons with wave vectors $\mathbf{k}$ in the different directions allowing emission and calculate their total spin moment $\mathbf{M}=n\mathbf{S}$, such that

$$\mathbf{M}=\int n(\mathbf{k})\mathbf{S}(\mathbf{k})\frac{d\Omega}{2\pi},\quad n=\int n(\mathbf{k})\frac{d\Omega}{2\pi} \tag{C4}$$

when entering the BBR after suffering the precession in the bulk crystal, given by integral (14) and its simplified form (15). We use the decomposition of the spin momentum $n(\mathbf{k})\mathcal{S}_0(\mathbf{k})$:

$$n(\mathbf{k})\mathcal{S}_0(\mathbf{k})=m_1\mathbf{z}+m_2\cos\theta\,\mathbf{z}' , \tag{C5}$$

where m_1 and m_2 are defined according to formulas (A22)–(A24) and only depend on k. We successively consider the emission from the (110) and (100) faces, and deduce the maximum polarization $P_0=2S=2M/n$. In the case of photoemission from the (110) face, the bulk precession angle θ_{bulk} is equal to $\arctan(M_x/M_z)=\arctan(S_x/S_z)$.

a. *Emission from the (110) surface*

We showed above in subsection 1 a that $M_y=0$. We express $\omega(\mathbf{k})$ in the $(\mathbf{x},\mathbf{y},\mathbf{z})$ frame with z along (110), as deduced from [Eq. (16)] (see Sec. III C 1), to calculate M_x and M_z. It is straightforward to see that the three components of $\mathbf{M}$ are

$$M_x=(\alpha l/4\pi)\lambda(m_1I_4+m_2I_5)\quad\text{with}\ \lambda=\omega_0 l/v , \tag{C6}$$

$$M_y=0 ,$$

$$M_z=(\alpha l/4\pi)[m_1(I_1+I_2)+m_2I_3] , \tag{C7}$$

where I_1, I_2, I_3, I_4, and I_5 are the dimensionless integrals defined below, φ being the azimuthal angle in the $(\mathbf{x},\mathbf{y},\mathbf{z})$ frame:

$$I_1=\int_0^{\pi/2}\int_0^{2\pi}\frac{1-(\boldsymbol{\omega}\cdot\mathbf{z}/\omega)^2}{1+(\omega l/v)^2}\sin\theta\cos\theta\,d\theta\,d\varphi , \tag{C8}$$

$$I_2=\int_0^{\pi/2}\int_0^{2\pi}(\boldsymbol{\omega}\cdot\mathbf{z}/\omega)^2\sin\theta\cos\theta\,d\theta\,d\varphi , \tag{C9}$$

$$I_3=\int_0^{\pi/2}\int_0^{2\pi}\frac{\sin\theta\cos^3\theta}{1+(\omega l/v)^2}d\theta\,d\varphi , \tag{C10}$$

$$I_4=\int_0^{\pi/2}\int_0^{2\pi}\frac{(\boldsymbol{\omega}\cdot\mathbf{y})/\omega_0}{1+(\omega l/v)^2}\sin\theta\cos\theta\,d\theta\,d\varphi , \tag{C11}$$

$$I_5=\int_0^{\pi/2}\int_0^{2\pi}\frac{(\boldsymbol{\omega},\mathbf{k},\mathbf{x})/\omega_0}{1+(\omega l/v)^2}\sin\theta\cos^2\theta\,d\theta\,d\varphi . \tag{C12}$$

Because of the complicated variation of $\omega(\mathbf{k})$ versus angle and energy, these integrals are calculated numerically.

b. *Emission from the (100) surface*

Using similar arguments, we find that

$$M_x=0 ,$$

$$M_y=0 , \tag{C13}$$

$$M_z=(\alpha l/4\pi)[m_1(I_1'+I_2')+m_2I_3'] ,$$

where I_1', I_2', and I_3' are, respectively, the same integrals as I_1, I_2, and I_3, except that the proper expression of $\omega(\mathbf{k})$, deduced from formula (7), is used. A reduction of M_z, i.e., of P_0, due to the presence of ω, is evidenced.

3. Precession in the band-bending region for the (110) face

We only consider the two special cases of electrons entering the BBR with spins along z (subsection 2 a), or of ballistic electrons excited from the Γ_{8h} heavy-hole band and having precessed in the bulk solid (subsection 2 b).

a. *Spins along z at $z=-\mathcal{L}$*

The precession is built up in the BBR. All spins precess in the x-z plane (see Sec. III A 1) and the total precession suffered in the BBR by an electron of momentum $\mathbf{k}_0$ at $z=-\mathcal{L}$, with $k_{z0}>0$, is [Eq. (21)]

$$\theta_B(\mathbf{k}_0)\approx\int_0^{\tau}\omega_y dt . \tag{C14}$$

Using the relation [Eq. (18)] between dt and dk_z, the fact that $k_z dk_z = k\,dk$, and the expression of ω_y [Eq. (16)], we get

$$\theta_B(\mathbf{k}_0)=2G(\varepsilon_0\varepsilon_r/N_Ae^2)^{1/2}\times\int_{k_0}^{k_1}a(k)b(k)\frac{k^2-k_0^2f(\theta,\varphi)}{[\varepsilon(k)-\varepsilon(k_0)]^{1/2}}dk , \tag{C15}$$

where φ is the azimuthal angle in the $(\mathbf{x},\mathbf{y},\mathbf{z})$ frame,

$$f(\theta,\varphi)=\sin^2\theta(2\sin^2\varphi+3\cos^2\varphi) , \tag{C16}$$

and k_1 is such that

$$\varepsilon(k_1)=\varepsilon(k_0)+\delta . \tag{C17}$$

The integral is performed numerically. The result for $\delta=0.6$ eV and k_0 corresponding to a kinetic energy $\varepsilon(k_0)=0.4$ eV is plotted in Fig. 14 for various angles (θ,φ).

To get a physical insight, we use the approximate expression (B18) of the kinetic energy for large momenta $\varepsilon(k_1)-\varepsilon(k_0)=A(k-k_0)$ valid in our energy range $1<k<3$ nm^{-1}. We also notice that in this range the product ab is almost constant (≈ 0.025). Under these two assumptions an analytical expression of $\theta_B(\mathbf{k}_0,\delta)$ is obtained:

$$\theta_B(\mathbf{k}_0,\delta)\approx 4GA^{-3}ab(\varepsilon_0\varepsilon_r/N_Ae^2)^{1/2}\times\delta^{5/2}([1-f(\theta,\varphi)]Y^2+\tfrac{2}{3}Y+\tfrac{1}{5}) , \tag{C18}$$

where $Y = Ak_0/\delta$. This expression shows that $\theta_B(\mathbf{k}_0,\delta)$ may be negative for large off-normal angles [$f(\theta,\varphi) > 1$] and an energy Ak_0 large with respect to δ. For example, in the case of Fig. 14 the approximate expression (C18) predicts that for $\varphi = 0$, $\theta_B = 0$ for $\theta = 48°$, whereas the exact calculation (C15) gives $\theta = 57°$.

The observed $\theta_B(k_0,\delta)$ is the average of $\theta_B(\mathbf{k}_0,\delta)$ over the momentum distribution at constant energy $\varepsilon(k_0)$ which enters the BBR. The only angle-dependent factor in (C18) is $f(\theta,\varphi)$, and its average for an isotropic distribution is $\frac{5}{3}$. The numerical value of $\theta_B(k_0)$ is plotted in Fig. 15 versus the kinetic energy $\varepsilon(k_0)$ for different BB energies δ. From the approximate expression (C18), we find an expression of $\theta_B(k_0,\delta)$ in reduced units, with a numerical expression [the angle $\theta_B(k_0,\delta)$ is in deg]

$$\theta_B(k_0,\delta) \approx 46.3 \times [\delta(\text{eV})]^{5/2}(-\tfrac{2}{3}Y^2 + \tfrac{2}{3}Y + \tfrac{1}{5}) . \quad \text{(C19)}$$

We deduce from (C19) that θ_B is minimum versus δ for $Ak_0/\delta \approx 3.4$ and that it is zero for $Ak_0/\delta \approx 1.25$. The curves $\theta_B(k_0,\delta)$ versus δ in Fig. 16 show minima which verify this latter relation with a maximum error of 16 meV in our energy range.

In the experiment the precession angle is measured for different kinetic energies ε of the emitted electrons on a sample of given BB energy δ. We expect θ_B to be a decreasing function of the energy, positive for small ε, then it becomes negative, as shown in Fig. 15. Practically, the measurement of the value of k_0 for which θ_B vanishes should give an estimate of δ.

b. Hot-electron distribution

The number (the total spin momentum) of ballistic electrons with momentum $\mathbf{k}$ reaching the $z = 0$ surface plane is given, in the approximation $\alpha l \ll 1$, by Eq. (12) [Eq. (15)] in which the integration is performed over the whole sample thickness ($-\infty < z \leq 0$). For electrons excited from the heavy-hole band [Eq. (A17)],

$$n(\mathbf{k}) = C(1+\cos^2\theta), \quad n(\mathbf{k})\mathbf{S}(\mathbf{k}) = -C\cos\theta\,\mathbf{z}' , \quad \text{(C20)}$$

so that the momentum at $z = 0$ is equal to

$$n(\mathbf{k})\mathbf{S}(\mathbf{k}) = -\frac{C\alpha l\cos^2\theta\,\mathbf{z}'}{1+(\omega l/v)^2} - \frac{C\alpha l\cos\theta}{1+(\omega l/v)^2}\frac{\omega l}{v}\left[\frac{\boldsymbol{\omega}\times\mathbf{z}'}{\omega}\right] . \quad \text{(C21)}$$

These results assume that the electrons undergo the same precession vector $\boldsymbol{\omega}(\mathbf{k})$ in the whole solid. In fact, because of the presence of the BBR, $\boldsymbol{\omega}(\mathbf{k})$ is constant for $-\infty < z < -\mathcal{L}$, and then becomes a function of the position. The correct calculation should use the value at $z = -\mathcal{L}$ for the spin momentum entering the BBR from the bulk crystal. To simplify the calculation, we will take the value at $z = 0$, i.e., $n(\mathbf{k})\mathbf{S}_b(\mathbf{k})$ as given by Eq. (C21). This means counting twice the precession in the BBR, once with the bulk constant vector $\boldsymbol{\omega}(\mathbf{k})$ and the second time with a precession vector increasing with z. In fact, the precession angle at constant $\boldsymbol{\omega}(\mathbf{k})$ on a distance $\mathcal{L}$, of the order $\omega_0\mathcal{L}/v$, is negligible with respect to the total bulk precession angle as long as $\mathcal{L} \ll l$: this is approximately the case for $\mathcal{L} \approx 300$ Å and the l value that we determine ($l \approx 1200$ Å). The net spin momentum $\mathbf{M} = n\mathbf{S}$ after crossing the BBR [see Eq. (21)] is calculated numerically. It depends on the parameter $\lambda = \omega_0 l/v$ and on the BB energy δ. We take for initial value of λ its determination from the polarization at maximum kinetic energy when the effect of the BBR is neglected. Then we try different values of δ compatible with the low- and intermediate-energy precession angles. We find that the additional precession angle due to the BBR ranges from $+7°$ to $+12°$, to be compared to bulk precession angles of the order of $20°-30°$ according to the excitation energy. This extra angle is *positive* since the hot-electron distribution favors momenta oriented close to the surface normal. In these same conditions the decrease of the net polarization in the BBR (from 24% to 19% for $\lambda = 2.5$ and from 18% to 17% for $\lambda = 3.2$, no significant effect for larger λ) is not very sensitive to the value of δ. Considering the experimental uncertainty, and the fact that the BBR contribution is overestimated, as mentioned above, we will finally take for θ_p and P_0 the *bulk* contributions calculated for $-\infty < z < 0$ according to the procedure of Sec. III C 1.

---

*Present address: Department ZFE FKE, Siemens A.G., Otto-Hahn-Ring, D-8000 München 83, West Germany.

[1]E. O. Kane, J. Phys. Chem. Solids **1**, 249 (1957).

[2]M. I. D'yakonov and V. I. Perel', Zh. Eksp. Teor. Fiz. **60**, 1954 (1971) [Sov. Phys.—JETP **33**, 1053 (1971)].

[3]For a review, see B. P. Zakharchenya, D. N. Mirlin, V. I. Perel', and I. I. Reshina, Usp. Fiz. Nauk **136**, 459 (1982) [Sov. Phys.—Usp. **25**, 143 (1982)].

[4]V. I. Safarov and A. N. Titkov, Physica B + C **117B & 118B**, 497 (1983).

[5]H. Riechert, S. F. Alvarado, A. N. Titkov, and V. I. Safarov, in *Proceedings of the 17th International Conference on the Physics of Semiconductors, San Francisco, 1984,* edited by J. D. Chadi and W. A. Harrison (Springer, New York, 1985), p. 1361.

[6]H.-J. Drouhin, C. Hermann, and G. Lampel, Phys. Rev. B **31**, 3872 (1985).

[7]H.-J. Drouhin, C. Hermann, and G. Lampel, Phys. Rev. B **31**, 3859 (1985).

[8]V. D. D'ymnikov, M. I. D'yakonov, and N. I. Perel', Zh. Eksp. Teor. Fiz. **71**, 2373 (1976) [Sov. Phys.—JETP **44**, 1252 (1976)].

[9]H. Riechert and S. F. Alvarado, in *Festkörperprobleme (Advances in Solid State Physics),* edited by P. Grosse (Vieweg, Braunschweig, 1985), Vol. XXV, p. 267.

[10]H.-J. Drouhin and M. Eminyan, Rev. Sci. Instrum. **57**, 1052 (1986).

[11]D. M. Campbell, C. Hermann, G. Lampel, and R. Owen, J. Phys. E **18**, 664 (1985).

[12]This formula derives from the integrated form of Ampère's

theorem and takes into account neither the dimension nor the exact voltage applied to the electron optics. Thus it can only give an order of magnitude of Θ or i_0.

[13]The uncertainty in the precession angle θ_p can be overestimated as follows: a convenient way to determine θ_p consists, in a position $\Phi=0$ of total compensation, of finding the external precession angle $\Theta=2\pi i/i_0$ [see Eq. (2)] for which $P(i)=0$, so that $\Theta=\pi/2-\theta_p-\Psi$. At this point $dP/d\Theta=-P_0$ and, as the cosine is nearly linear in this region, the slope can also be written $-\Delta P/\Delta\Theta$. Then $\Delta\theta_p(\text{rad})\sim\Delta P/|P_0|$.

[14]See, for instance, J. R. Chelikowski and M. L. Cohen, Phys. Rev. B **14**, 556 (1976); N. E. Christensen, *ibid.*, **30**, 5753 (1984).

[15]See, for instance, R. A. Smith, *Semiconductors* (Cambridge University Press, London, 1961), Chap. 4.

[16]Sh. M. Kogan, A. D. Korinfskii, A. L. Musatov, A. F. Polupanov, and S. V. Geizer, Izv. Akad. Nauk SSSR, Ser. Fiz. **49**, 1745 (1985) [Bull. Acad. Sci. USSR, Phys. Ser. **49**, 977 (1985)].

[17]J. S. Blakemore, J. Appl. Phys. **53**, R123 (1982).

[18]For a review, see *Optical Orientation,* Vol. 8 of *Modern Problems in Solid State Sciences,* edited by F. Meier and B. P. Zakharchenya (Elseiver, Amsterdam, 1984).

[19]N. E. Christensen and M. Cardona, Solid State Commun. **51**, 491 (1984).

[20]G. F. Koster, J. O. Dimmock, R. G. Wheeler, and H. Statz, *Properties of the Thirty-Two Points Groups* (MIT Press, Cambridge, Mass., 1963).

[21]V. A. Marushchak, M. N. Stepanova, and A. N. Titkov, Fiz. Tverd. (Leningrad), **25**, 3537 (1983) [Sov. Phys.—Solid State **25**, 2035 (1983)].

[22]H.-J. Drouhin, C. Hermann, and G. Lampel, in *Festkörperprobleme (Advances in Solid State Physics),* Ref. 9, Vol. XXV, p. 255.

[23]G. Fishman and G. Lampel, Phys. Rev. B **16**, 820 (1977).

[24]J. H. Pollard, in *Proceedings of the Second European Electro-Optics Markets and Technology Conference, Montreux, 1974,* edited J. Walker (Mack Brooks Exhibitions, Ltd., St. Albans, 1974), p. 316.

[25]D. T. Pierce and F. Meier, Phys. Rev. B **13**, 5484 (1976).

[26]W. Mönch, Surf. Sci. **132**, 92 (1983).

[27]We do not take into account the selection rule of conservation of the wave-vector component parallel to the surface: Indeed, following the method indicated by Bell in *Negative Electron Affinity Devices* (Clarendon, Oxford, 1973) [see also M. G. Burt and J. C. Inkson, J. Phys. D **8**, L3 (1975)], emission of L electrons from the (110) face is forbidden [as well as for (100) face]. Yet we observe an L structure in the EDC's probably because this conservation law is relaxed in the presence of Cs [G. W. Gobeli, F. G. Allen, and E. O. Kane, Phys. Rev. Lett. **12**, 94 (1964)].

[28]E. O. Kane, in *Semiconductors and Semimetals,* edited by R. K. Willardson and A. C. Beer (Academic, New York, 1966), Vol. 1, p. 75.

[29]C. Hermann, H.-J. Drouhin, and H. Riechert, in *Proceedings of the Nineteenth International Conference on the Physics of Semiconductors, Warsaw, 1988,* edited by M. Grynberg (Springer, New York, 1988).

[30]M. G. Burt and J. C. Inkson, J. Phys. D **9**, L5 (1976).

[31]These numbers somewhat differ from those given in a previous paper by H.-J. Drouhin, C. Hermann, and G. Lampel, [Phys. Rev. B **31**, 3872 (1985)], where, to simplify, a velocity deduced from the parabolic-band model had been used over the whole energy range.

[32]M. I. D'yakonov, V. I. Perel', and I. N. Yassevich, Fiz. Tekh. Poluprovodn. **11**, 1364 (1977) [Sov. Phys.—Semicond. **11**, 801 (1977)].

[33]D. Neilson, J. Szymanski, and D.-X. Lu, in *Proceedings of the Third International Conference on Modulated Semiconductor Structures,* Montpellier, France, 1987, edited by A. Raymond and P. Voisin [J. Phys. (Paris) Colloq. **48**, C5-263 (1987)].

[34]G. Dresselhaus, Phys. Rev. **100**, 580 (1955).

[35]C. Hermann and C. Weisbuch, Phys. Rev. B **15**, 823 (1977).

[36]In this three-band expression of m^*, we use the correct value of P in GaAs as determined by C. Hermann and C. Weisbuch [Phys. Rev. B **15**, 823 (1977)]. Since the accurate prediction of m^* requires a five-band description, the value calculated from expression (B7) differs from the experimental one.

[37]W. Zawadzki, P. Pfeffer, and H. Sigg, Solid State Commun. **53**, 777 (1985).

[38]A. G. Aronov, G. E. Pikus, and A. N. Titkov, Zh. Eksp. Teor. Fiz. **84**, 1170 (1983) [Sov. Phys.—JETP **57**, 680 (1983)].